This document is an excerpt of from Brannon's unpublished working document that was later partially transcribed in the following two publications:

Brannon, R. M. and S. Leelavanichkul (2010) A multi-stage return algorithm for solving the classical damage component of constitutive models for rocks, ceramics, and other rock-like media. *Int. J. Fracture* v. **163**(1), pp. 133-149.

K.C. Kamojjala, R. Brannon, A. Sadeghirad, and J. Guilkey (2013) Verification tests in solid mechanics, Engineering with Computers, 1-21.

Unfortunately, both of those publications had some solution transcription typos, which were not in this original working document.

Equation (3.129) of this excerpt document has correct formulas (and additional details) that serve as errata for the two publications. We apologize for the inconvenience that our typos might have caused, and we are grateful to Dr. Andy Tonge for bringing them to our attention!
Be advised: since this is an excerpt from a larger document, there are some references to governing equations that have not been included in this excerpt, but which are the same governing equations summarized in the publications.

EXACT integration of non-hardening Von Mises plasticity models subjected to a constant strain rate with a time-varying tangent stiffness

The previous section presented analytical results for special loading paths that would ensure that neither the principal stress directions nor the Lode angle of the stress (i.e., the angular position on the circular octahedral yield profile) would never vary during plastic loading, which meant that the yield normal would be constant and therefore the tangent stiffness tensor would be constant. In that case, a piecewise linear strain history results in a piecewise linear stress response through direct application of Eq. 2.22. Here in this section, we derive results for piecewise constant strain rate problems that result in rotation of the stress deviator. Of course, for von Mises plasticity, the magnitude of the stress deviator is constant. Hence, rotation of the stress deviator is actually motion on a sphere embedded in the five-dimensional space of deviatoric symmetric tensors. In this very abstract geometrical perspective, we will show that the stress moves along a major circumference of the sphere to align itself toward the constant applied strain rate deviator. We will show that the angle between the strain rate and stress deviator decays exponentially to zero.

For nonhardening associative Von Mises plasticity, the first-order ODE governing the unit tensor in the direction of the stress deviator is given in Eq. __:

$$\dot{\underset{\approx}{N}} = \dot{\underset{\approx}{U}} - \underset{\approx}{N}(\underset{\approx}{N}:\dot{\underset{\approx}{U}}), \qquad \text{where } \dot{U} = \frac{2G\dot{\gamma}}{\sqrt{2}\tau_y}$$

$$\text{subject to } \underset{\approx}{N} = \underset{\approx}{N}_0 \text{ when } t = t_0 \tag{3.73}$$

Here, G is the shear modulus, τ_y is the yield in shear, and $\dot{\underset{\approx}{\gamma}}$ is the deviatoric part of the applied strain rate. To ensure that the material behavior is plastic for $t > t_0$, the initial stress state must lie on the yield surface and the strain rate must be directed outward from the yield surface (i.e., $\underset{\approx}{N}_0 : \dot{\underset{\approx}{U}} > 0$). During plastic intervals when the strain rate deviator $\dot{\underset{\approx}{\gamma}}$ is held constant, the exact solution may be evaluated at any time t via the following algorithm (proof provided afterward):

STEP 0: Decompose the problem into isotropic and deviatoric parts.

Given a stress state $\underset{\approx}{\sigma}_0$ that resides on the yield surface at time $t=t_0$, and given a total strain rate $\dot{\underset{\approx}{\varepsilon}}$ that is held constant for $t > t_0$, compute

$$p_0 = \tfrac{1}{3}(\mathrm{tr}\underset{\approx}{\sigma}_0) \qquad \text{and} \qquad \underset{\approx}{S}_0 = \underset{\approx}{\sigma}_0 - p_0\underset{\approx}{I} \tag{3.74}$$

$$\dot{\varepsilon}_v = \mathrm{tr}\dot{\underset{\approx}{\varepsilon}} \qquad \text{and} \qquad \dot{\underset{\approx}{\gamma}} = \dot{\underset{\approx}{\varepsilon}} - \tfrac{1}{3}\dot{\varepsilon}_v\underset{\approx}{I} \tag{3.75}$$

The time varying solution for mean stress is found immediately by

$$p(t) = p_0 + K\dot{\varepsilon}_v(t - t_0) \tag{3.76}$$

First check if the strain rate deviator happens to point in the same direction as $\underset{\approx}{S}_0$. Specifically, if

$$\dot{\underset{\approx}{\gamma}} - \frac{\underset{\approx}{S}_0(\underset{\approx}{S}_0 : \dot{\underset{\approx}{\gamma}})}{2\tau_y^2} = \underset{\approx}{0} \tag{3.77}$$

then the stress deviator is constant, and the final solution for the time-varying stress is simply $\underset{\approx}{\sigma} = \underset{\approx}{\sigma}_0 + K\dot{\varepsilon}_v(t - t_0)\underset{\approx}{I}$. Otherwise, the stress deviator is changing direction and the remainder of this algorithm must be followed.

STEP 1: Compute "helper" constants. The following constant scalars and tensors can be computed from the constant parameters in the problem statement. They may, therefore, be computed once and saved.

$$\underset{\approx}{N}_0 = \frac{\underset{\approx}{S}_0}{\sqrt{2}\tau_y} \qquad \text{Unit tensor in the direction of the initial stress deviator} \qquad (3.78)$$

$$\dot{\gamma} = \left\|\dot{\underset{\approx}{\gamma}}\right\| = \sqrt{\dot{\gamma}_{ij}\dot{\gamma}_{ij}} \qquad \text{magnitude of the total strain rate deviator} \qquad (3.79)$$

$$\alpha = \frac{\sqrt{2}\tau_y}{2G} \qquad \text{a non-dimensional "helper" parameter} \qquad (3.80)$$

(to obtain an orthogonal basis for the span of $\dot{\underset{\approx}{\gamma}}$ and $\underset{\approx}{N}_0$) as follows

$$\underset{\approx}{E}_1 = \dot{\underset{\approx}{\gamma}}/\dot{\gamma} \qquad \text{Unit tensor in the direction of the strain rate deviator} \qquad (3.81)$$

$$n_{01} = \underset{\approx}{N}_0 : \underset{\approx}{E}_1 \qquad (3.82)$$

$$\underset{\approx}{E}_2 = \frac{\underset{\approx}{N}_0 - (n_{01})\underset{\approx}{E}_1}{\sqrt{1-(n_{01})^2}} \qquad (3.83)$$

Remark: $\underset{\approx}{E}_1$ and $\underset{\approx}{E}_2$ form an orthonormal pair resulting from Gram-Schmidt orthogonalization of $\dot{\underset{\approx}{\gamma}}$ and $\underset{\approx}{N}_0$. The check in Eq. __ ensures that this part of the algorithm is skipped if $\dot{\underset{\approx}{\gamma}}$ and $\underset{\approx}{N}_0$ are parallel. Consequently, division by zero in Eq. __ is impossible.

STEP 2: Evaluate time-varying part of the solution. For $t > t_o$,

$$\gamma(t) = \gamma_0 + \dot{\gamma}(t - t_o) \qquad (3.84)$$

$$T(t) \equiv \frac{1+n_{01}}{1-n_{01}} \exp\left[\frac{2\dot{\gamma}(t-t_o)}{\alpha}\right] \qquad (3.85)$$

$$\boxed{\underset{\approx}{N}(t) = \frac{(T-1)\underset{\approx}{E}_1 + (2\sqrt{T})\underset{\approx}{E}_2}{T+1}} \qquad [T = T(t)] \qquad (3.86)$$

Stress deviator: $\underset{\approx}{S}(t) = \sqrt{2}\tau_y \underset{\approx}{N}(t)$ (3.87a)

Mean stress: $p(t) = p_0 + K\dot{\varepsilon}_v(t - t_0)$ (3.87b)

Total stress: $\underset{\approx}{\sigma}(t) = \underset{\approx}{S}(t) + p(t)\underset{\approx}{I}$ (3.87c)

STEP 3 (optional): Evaluate the decaying angle between the stress deviator

and the strain rate deviator. The time varying angle θ between the stress deviator and the constant strain rate can be computed by

$$\theta = \tan^{-1}\left(\frac{2\sqrt{T}}{T-1}\right) \qquad [T = T(t)] \tag{3.88}$$

This angle is plotted in Fig. 3.6. As time progresses, the stress deviator changes orientation to become progressively aligned with the constant strain rate $(\theta \to 0)$.

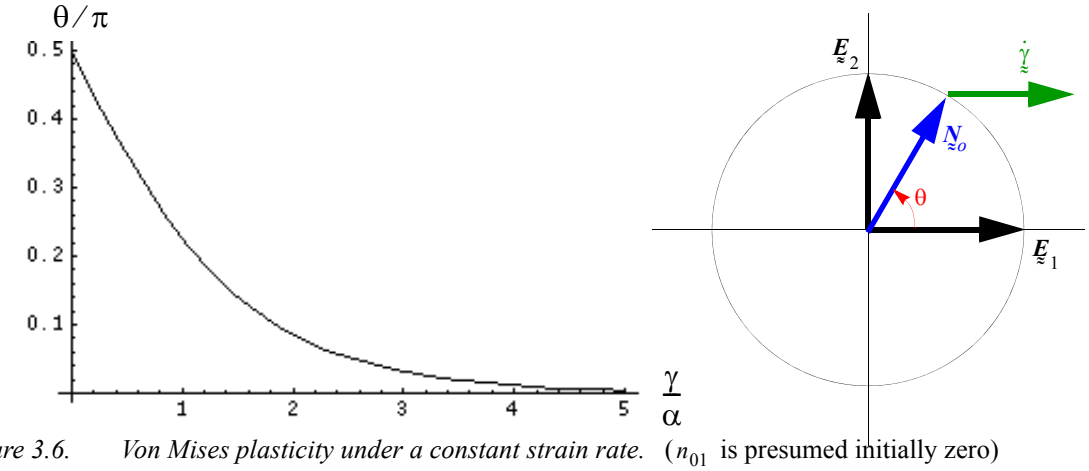

Figure 3.6. Von Mises plasticity under a constant strain rate. (n_{01} is presumed initially zero)

STEP 4 (optional): Plastic strain. The plastic strain rate and its magnitude are

$$\dot{\underset{\approx}{\varepsilon}}^p = \dot{\gamma}^p \underset{\approx}{N} \quad \text{where} \quad \dot{\gamma}^p = \left\| \dot{\underset{\approx}{\varepsilon}}^p \right\| = \left(\frac{T-1}{T+1}\right)\dot{\gamma} \tag{3.89}$$

A scalar measure of the overall "plastic strain" (i.e., the integral of $\dot{\gamma}^p$ over time) is

$$\gamma^p = \gamma_0^p + \alpha \ln[\tfrac{1}{2}(1+T)(1-n_{01})] - \dot{\gamma}(t-t_o), \tag{3.90}$$

or

$$\gamma^p - \gamma_0^p = \alpha \ln\left\{\frac{1-n_{01}+(1+n_{01})\exp\left[\frac{2\dot{\gamma}(t-t_o)}{\alpha}\right]}{2}\right\} - \dot{\gamma}(t-t_o), \tag{3.91}$$

where γ_0^p is the initial value of γ^p at time t_0.

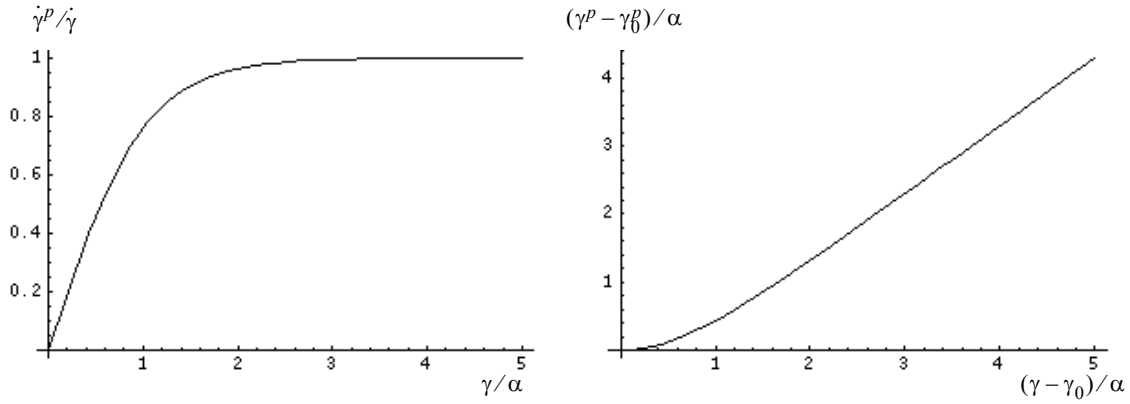

Figure 3.7. Plastic strain for the Von Mises response under a constant strain rate. The first plot shows the ratio of the plastic strain rate to the total strain rate, plotted as a function of the total strain magnitude (normalized by the factor $\alpha \equiv (\sqrt{2}k)/(2G)$). The second plot shows the "plastic strain" (normalized by α). These plots assume $n_{01} = 0$.

PROOF. Now we will prove the exact Von Mises integration presented above. The proof is included here only for completeness -- it does not lend much insight into the problem.

The ODE to be solved is

$$\dot{\underset{\approx}{N}} = \dot{\underset{\approx}{U}} - \underset{\approx}{N}(\underset{\approx}{N}:\dot{\underset{\approx}{U}}) \text{, where } \dot{\underset{\approx}{U}} = \text{constant}$$

$$\text{subject to } \underset{\approx}{N} = \underset{\approx}{N}_o \text{ when } t = t_o \tag{3.92}$$

Any symmetric and deviatoric tensor has five independent components. Furthermore, knowing that $\underset{\approx}{N}$ is a unit tensor tells us that the time varying solution for $\underset{\approx}{N}$ will always lie on the four-dimensional surface of a five dimensional unit sphere. We show in this section that $\underset{\approx}{N}$ will move along the major diameter of the sphere, starting at its known initial orientation, $\underset{\approx}{N}_0$, and asymptotically approaching an orientation aligned with $\dot{\underset{\approx}{U}}$.

Visualizing *five-dimensional* space is difficult. *Two-dimensional* space is far easier. Knowing that this problem involves two known tensors, $\dot{\underset{\approx}{U}}$ and $\underset{\approx}{N}_0$, it makes sense to set up an orthonormal basis for tensor space in which the first two base tensors span the same plane as our two known tensors. It will be shown that all motion of the stress deviator (and therefore motion of $\underset{\approx}{N}$) will occur entirely within this 2D subspace.

First introduce a basis for which the first base tensor, $\underset{\approx}{E}_1$, is the unit tensor in the direction of $\dot{\underset{\approx}{U}}$ (which is identical to a unit tensor in the direction of $\dot{\underset{\approx}{\gamma}}$)

$$\underset{\approx}{E}_1 = \frac{\dot{\underset{\approx}{U}}}{\dot{\upsilon}}, \text{ where } \dot{\upsilon} \equiv \sqrt{\dot{\underset{\approx}{U}}:\dot{\underset{\approx}{U}}} = \frac{2G}{\sqrt{2}\tau_y}\left\|\dot{\underset{\approx}{\gamma}}\right\| \tag{3.93}$$

Because $\dot{\underset{\approx}{U}}$ has been assumed constant, both $\dot{\upsilon}$ and $\underset{\approx}{E}_1$ may be treated as known constants.

The time-varying $\underset{\sim}{N}$ can always be decomposed into a part that is parallel to $\underset{\sim}{E}_1$ plus a remainder that is perpendicular to $\underset{\sim}{E}_1$. Namely, we can always write

$$\underset{\sim}{N}(t) = n_1(t)\underset{\sim}{E}_1 + \underset{\sim}{\mu}(t) \tag{3.94}$$

where

$$n_1 = \underset{\sim}{N} : \underset{\sim}{E}_1 \tag{3.95}$$

and

$$\underset{\sim}{\mu} = \underset{\sim}{N} - \underset{\sim}{E}_1(\underset{\sim}{E}_1 : \underset{\sim}{N}) \tag{3.96}$$

With this decomposition, the governing equation, 3.92, becomes

$$\dot{n}_1\underset{\sim}{E}_1 + \dot{\underset{\sim}{\mu}} = \upsilon\underset{\sim}{E}_1 - (n_1\underset{\sim}{E}_1 + \underset{\sim}{\mu})[(n_1\underset{\sim}{E}_1 + \underset{\sim}{\mu}) : \dot{\upsilon}\underset{\sim}{E}_1] \tag{3.97}$$

Not only is $\underset{\sim}{\mu}$ perpendicular to $\underset{\sim}{E}_1$ by construction, but (because $\underset{\sim}{E}_1$ is constant) so is $\dot{\underset{\sim}{\mu}}$. The part of the above equation that is perpendicular to $\underset{\sim}{E}_1$ is given by

$$\dot{\underset{\sim}{\mu}} = -\underset{\sim}{\mu}[\dot{\upsilon}N_1] \tag{3.98}$$

This result shows that the rate of $\underset{\sim}{\mu}$ is always proportional to $\underset{\sim}{\mu}$ itself. This is possible only if the *direction* of $\underset{\sim}{\mu}$ remains constant. We will define $\underset{\sim}{E}_2$ to equal this constant direction. Since the direction of $\underset{\sim}{\mu}$ is constant, it must equal the *initial* direction of $\underset{\sim}{\mu}$ obtained by evaluating Eq. 3.96 at time t_o, and then normalizing the result. Hence, we define

$$\underset{\sim}{E}_2 \equiv \frac{\underset{\sim}{N}_o - \underset{\sim}{E}_1(\underset{\sim}{E}_1 : \underset{\sim}{N}_o)}{\left\| \underset{\sim}{N}_o - \underset{\sim}{E}_1(\underset{\sim}{E}_1 : \underset{\sim}{N}_o) \right\|} = \frac{\underset{\sim}{N}_o - \underset{\sim}{E}_1(n_1^0)}{\sqrt{1-(n_1^0)^2}} \tag{3.99}$$

Since we have now shown that $\underset{\sim}{\mu}$ can be expressed as a linear combination of $\underset{\sim}{E}_1$ and $\underset{\sim}{E}_2$, Eq. 3.94 shows that the time varying unit normal $\underset{\sim}{N}(t)$ must also be expressible as a combination of these two tensors:

$$\underset{\sim}{N}(t) = n_1(t)\underset{\sim}{E}_1 + n_2(t)\underset{\sim}{E}_2 \tag{3.100}$$

and the governing equation becomes

$$\dot{n}_1\underset{\sim}{E}_1 + \dot{n}_2\underset{\sim}{E}_2 = \dot{\upsilon}\underset{\sim}{E}_1 - [n_1\underset{\sim}{E}_1 + n_2\underset{\sim}{E}_2](\dot{\upsilon}n_1) \tag{3.101}$$

Equating coefficients of $\underset{\approx}{\boldsymbol{E}}_1$ and $\underset{\approx}{\boldsymbol{E}}_2$, gives a set of equations that must be solved simultaneously:

$$\dot{n}_1 = \dot{\upsilon}(1 - n_1^2) \tag{3.102}$$

$$\dot{n}_2 = -\dot{\upsilon} n_1 n_2 \tag{3.103}$$

To ensure that the final result is a unit tensor, we know that $n_1^2 + n_2^2 = 1$. Hence, it is natural to introduce an angle θ defined such that $n_1 = \cos\theta$ and $n_2 = \sin\theta$. For now, however, we will continue to use the Cartesian components n_1 and n_2. For the special case that $n_1 = 1$, the normal $\underset{\approx}{\boldsymbol{N}}$ would be aligned with the unit tensor $\underset{\approx}{\boldsymbol{E}}_1$ and the above equations would predict zero for the rates $\dot{n}_1$ and $\dot{n}_2$. This is the "trivial" solution. Physically, it means that a strain rate pointing in the same direction as the stress deviator will not change the stress deviator (i.e., it can't be pushed outside the von Mises cylinder, so it just stays put).

The interesting (nontrivial) solution corresponds to $n_1 \neq 1$. Under this assumption Eq. 3.103a may be integrated directly as follows:

$$\int \frac{dn_1}{(1 - n_1^2)} = \int \dot{\upsilon} dt \tag{3.104}$$

The result is

$$\frac{1 + n_1}{1 - n_1} = Ce^{2\dot{\upsilon}(t - t_o)} \tag{3.105}$$

where the integration constant is

$$C = \frac{1 + n_1^o}{1 - n_1^o} \tag{3.106}$$

This solution *asymptotes* towards $\underset{\approx}{\boldsymbol{N}} \to \underset{\approx}{\boldsymbol{E}}_1$ as time goes to infinity. Thus we see that the exact time varying solution for $\underset{\approx}{\boldsymbol{N}}$ always proceeds along the shortest path in stress space that will move $\underset{\approx}{\boldsymbol{N}}$ towards alignment with $\underset{\approx}{\boldsymbol{E}}_1$. Of course, for our fully plastic assumption to hold, the initial value n_1^o must be positive (otherwise, the solution will need to begin with an elastic phase during with the stress proceeds along a path parallel to $\underset{\approx}{\boldsymbol{E}}_1$ until the yield surface is reached. Consequently, the smallest possible value for the integration constant C is 1.

Solving Eq. 3.105 for n_1 gives

$$n_1 = \frac{T-1}{T+1}, \text{ where } T \equiv \frac{1+n_1^o}{1-n_1^o} e^{2\dot{\upsilon}(t-t_o)} \tag{3.107}$$

and, since $n_2 = \sqrt{1-n_1^2}$, we have

$$n_2 = \frac{2\sqrt{T}}{T+1} \tag{3.108}$$

Thus, the exact solution for the time varying unit normal is

$$\boxed{\underset{\approx}{\boldsymbol{N}} = \frac{(T-1)\underset{\approx}{\boldsymbol{E}}_1 + (2\sqrt{T})\underset{\approx}{\boldsymbol{E}}_2}{T+1}} \tag{3.109}$$

Having this exact solution available for the case of constant strain rates is handy for verifying numerical implementations. To visualize the solution, it's useful to define the angle that $\underset{\approx}{\boldsymbol{N}}$ makes with $\underset{\approx}{\boldsymbol{E}}_1$:

$$\theta = \tan^{-1}\left(\frac{n_2}{n_1}\right) = \tan^{-1}\left(\frac{2\sqrt{T}}{T-1}\right) \tag{3.110}$$

By definition, the plastic strain rate is computed as

$$\dot{\underset{\approx}{\varepsilon}}^p = \dot{\underset{\approx}{\varepsilon}} - \dot{\underset{\approx}{\varepsilon}}^e = \dot{\underset{\approx}{\gamma}} - \frac{\dot{\underset{\approx}{\boldsymbol{S}}}}{2G} = \frac{\sqrt{2}\tau_y}{2G}[\dot{\underset{\approx}{\boldsymbol{U}}} - \dot{\underset{\approx}{\boldsymbol{N}}}] = \frac{\sqrt{2}\tau_y}{2G}[\underset{\approx}{\boldsymbol{N}}(\underset{\approx}{\boldsymbol{N}}:\dot{\underset{\approx}{\boldsymbol{U}}})]$$

$$= \left\|\dot{\underset{\approx}{\gamma}}\right\|[\underset{\approx}{\boldsymbol{N}}(\underset{\approx}{\boldsymbol{N}}:\underset{\approx}{\boldsymbol{E}}_1)] = \left\|\dot{\underset{\approx}{\gamma}}\right\|\left(\frac{T-1}{T+1}\right)\underset{\approx}{\boldsymbol{N}} = \dot{\gamma}\left(\frac{T-1}{T+1}\right)\underset{\approx}{\boldsymbol{N}} \tag{3.111}$$

The magnitude of the plastic strain rate is

$$\dot{\gamma}^p = \left\|\dot{\underset{\approx}{\varepsilon}}^p\right\| = \left(\frac{T-1}{T+1}\right)\dot{\gamma} \tag{3.112}$$

Integrating this over time gives

$$\gamma^p \equiv \int_{t_o}^{t} \dot{\gamma}^p dt = \int_0^{\gamma} \frac{\dot{\gamma}^p}{\dot{\gamma}} d\gamma = \alpha\left\{\ln\left[\frac{1}{2}(1+\tau)(1-N_1^o)\right] - \upsilon\right\} \tag{3.113}$$

EXAMPLE. The exact solution presented above applies to non-hardening Von Mises plasticity for *any* constant strain rate that is not aligned with the yield normal. The solution applies even when the constant strain rate has time varying principal directions. However, to illustrate how the preceding exact algorithm is applied, we will consider here a simple a piecewise linear strain table in which the strain eigenvectors are fixed. The first leg, triaxial extension (TXE), brings the stress to yield. The second leg veers away from the TXE state into other Lode angles. The problem parameters are shown in Tables 3.1 and 3.2.

Table 3.1: Material parameters

name	symbol	value
yield in shear	τ_y	165 MPa
shear modulus	G	79 GPa

Table 3.2: Strain table

time (s)	ε_{11}	ε_{22}	ε_{33}
0	0	0	0
1	-0.003	-0.003	0.006
2	-0.0103923	0	0.0103923

During the initial loading, the strain rate is $\dot{\underset{\approx}{\gamma}} = \text{DIAG}[-0.003, -0.003, 0.006]$. Therefore, the stress rate is

$$\dot{\underset{\approx}{S}} = 2G\dot{\underset{\approx}{\gamma}} = \text{DIAG}[-474, -474, 948] \text{ GPa/s} \tag{3.114}$$

Integrating this constant stress rate over time gives

$$\underset{\approx}{S} = \text{DIAG}[-474, -474, 948](t) \text{ GPa} \qquad 0 < t < 0.201 \text{ s} \tag{3.115}$$

The limit time of 0.201 seconds marks the time at which this elastic solution reaches the yield surface. This yield time is found by setting

$$\underset{\approx}{S}:\underset{\approx}{S} = 2\tau_y^2 \tag{3.116}$$

and solving for t to obtain:

$$t^{\text{yield}} = 0.201 \text{ s} \tag{3.117}$$

For the remainder of this first leg, the stress remains constant because the strain rate and the stress are parallel. Specifically, for $t^{\text{yield}} < t < 1$,

$$\underset{\approx}{\boldsymbol{S}} = \text{DIAG}[-95.26, -95.26, 190.5] \quad \text{GPa} \qquad 0.201 < t < 1 \quad \text{s} \tag{3.118}$$

After yield is reached, the plastic strain rate equals the total strain rate. Therefore, the accumulated plastic strain rate during the leg is

$$\gamma^p = \dot{\gamma}(t - t^{\text{yield}}), \text{ where } \dot{\gamma} = 0.00734847 \qquad 0.201 < t < 1 \quad \text{s} \tag{3.119}$$

When the strain rate changes direction, launching the second leg of deformation, the stress and strain rate are no longer parallel, so the exact Von Mises algorithm applies. The constant strain rate over this leg is

$$\underset{\approx}{\dot{\gamma}} = \text{DIAG}[-0.00739, 0.003, 0.00439] \tag{3.120}$$

Starting with Eq. 3.78, the algorithm calls for computation of some "helper" quantities:

$$\underset{\approx}{\boldsymbol{N}}_0 = \frac{\underset{\approx}{\boldsymbol{S}}_0}{\sqrt{2}\tau_y} = \frac{1}{\sqrt{6}}\text{DIAG}[-1, -1, 2] \tag{3.121}$$

$$\dot{\gamma} = 0.0091706 \tag{3.122}$$

$$\alpha = 0.00147687 \tag{3.123}$$

$$\underset{\approx}{\boldsymbol{E}}_1 = \text{DIAG}[-0.811712, 0.329415, 0.482297] \tag{3.124}$$

$$n_{01} = 0.59069 \tag{3.125}$$

$$\underset{\approx}{\boldsymbol{E}}_2 = \frac{\underset{\approx}{\boldsymbol{N}}_0 - (n_{01})\underset{\approx}{\boldsymbol{E}}_1}{\sqrt{1-(n_{01})^2}} = \text{DIAG}[0.0882664, -0.747096, 0.65883] \tag{3.126}$$

The algorithm states that the time varying part of the solution is given by

$$T(t) \equiv \frac{1+n_{01}}{1-n_{01}}\exp\left[\frac{2\dot{\gamma}(t-t_o)}{\alpha}\right] = 3.88628e^{12.33(t-1)} \tag{3.127}$$

from which the stress deviator is then found by

$$\underset{\approx}{\boldsymbol{S}}(t) = \sqrt{2}\tau_y\left[\frac{(T-1)\underset{\approx}{\boldsymbol{E}}_1 + (2\sqrt{T})\underset{\approx}{\boldsymbol{E}}_2}{T+1}\right] \tag{3.128}$$

This is also the solution for total stress because the strain is traceless at all times (making the pressure zero). Thus, after substituting Eqs. 3.124, 3.126, and 3.127 into Eq. 3.128, the exact solution for the stress is

$$\sigma_{11} = \begin{cases} -474.0t & \text{if} \quad 0 < t \le 0.200976 \\ -95.26 & \text{if} \quad 0.200976 < t \le 1 \\ \dfrac{189.4 + 0.1704\sqrt{e^{12.33t}} + (-0.003242)e^{12.33t}}{1 + (0.00001712)e^{12.33t}} & \text{if} \quad 1 < t \le 2 \\ \to -189.409 & \text{as} \quad t \to \infty \end{cases} \text{MPa} \tag{3.129a}$$

$$\sigma_{22} = \begin{cases} -474.0t & \text{if} \quad 0 < t \le 0.200976 \\ -95.26 & \text{if} \quad 0.200976 < t \le 1 \\ \dfrac{-76.87 - 1.4425\sqrt{e^{12.33t}} + 0.001316e^{12.33t}}{1 + (0.00001712)e^{12.33t}} & \text{if} \quad 1 < t \le 2 \\ \to 76.867 & \text{as} \quad t \to \infty \end{cases} \text{MPa} \tag{3.129b}$$

$$\sigma_{33} = \begin{cases} 948.0t & \text{if} \quad 0 < t \le 0.200976 \\ 190.5 & \text{if} \quad 0.200976 < t \le 1 \\ \dfrac{-112.5 + 1.272\sqrt{e^{12.33t}} + 0.0019263e^{12.33t}}{1 + (0.00001712)e^{12.33t}} & \text{if} \quad 1 < t \le 2 \\ \to 112.542 & \text{as} \quad t \to \infty \end{cases} \text{MPa} \tag{3.129c}$$

To update the time-varying equivalent plastic strain γ^p, the initial value for the second leg is given by γ^p at the end of the *first* leg, which is found by evaluating Eq. 3.119 at time $t = 1$ to obtain

$$\gamma_0^p = 0.0058716 \tag{3.130}$$

Then the exact solution for plastic strain is obtained by applying Eq. 3.91 to obtain

$$\gamma^p = \begin{cases} 0 & \text{if} \quad 0 < t \le 0.200976 \\ 7.348t - 1.477 & \text{if} \quad 0.200976 < t \le 1 \\ 14.98 - 9.1076t + 1.4769\ln[0.2047 + 3.503 \times 10^{-6}e^{12.33t}] & \text{if} \quad 1 < t \le 2 \end{cases} \tag{3.131}$$

These solutions for the stress and plastic strain history are shown in Fig. 3.8.

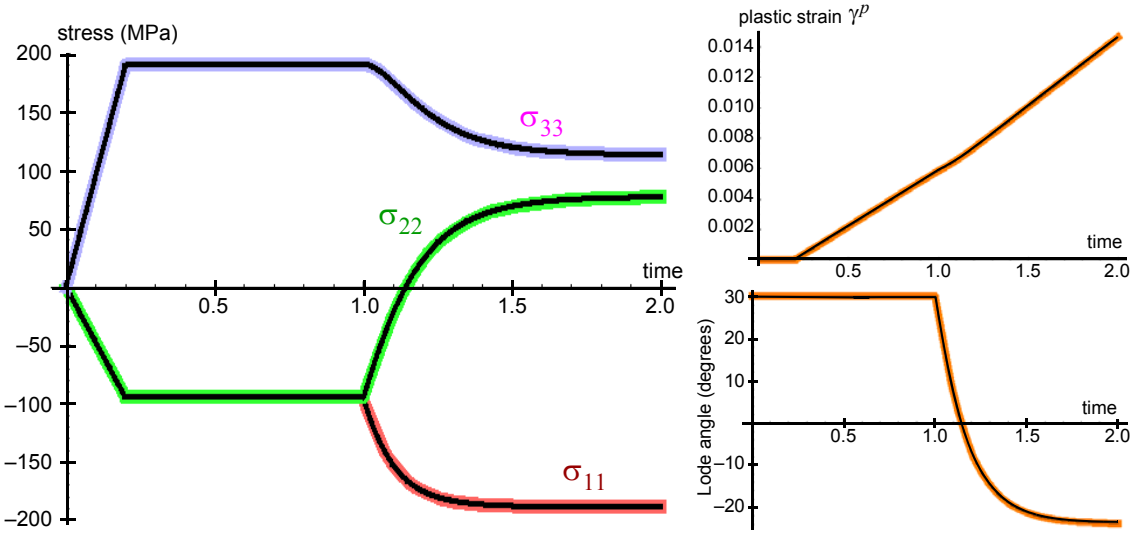

Figure 3.8. Exact solution to the Von Mises plasticity problem defined in Tables 3.1 and 3.2. The thick colored lines are the analytical solution. The thin black lines that overlay the exact solution are results from a numerical plasticity code that was verified against these analytical results.

A VERY SIMPLE VON MISES PROBLEM THAT OFTEN UNCOVERS POTENTIAL FOR DIVISION BY ZERO IN PLASTICITY CODES

Many plasticity codes include an implicit presumption that the total strain rate is nonzero whenever plasticity applies. Although this is true in most realistic applications, a simple verification test problem can be designed such that the trial stress history has a cubic time dependence such that the inflection point (where the trial elastic stress rate and its second time derivative are both zero) is reached at the precise moment that yield is reached. Often, plasticity models can be made to produce gargantuan errors (or division by zero) in scenarios like this, making this type of loading worth including in any simple benchmarking suite.

4. Analytical single-element solutions for Drucker-Prager plasticity

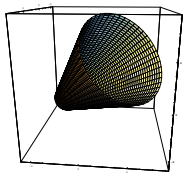

The yield function for linear Drucker-Prager plasticity is

$$f = \frac{r}{r_0} + \frac{z}{z_0} - 1 \tag{4.1}$$

Alert: *r* and *z* are respectively defined as *r* = sqrt(2 J_2) = magnitude of the stress deviator and *z* = I_1/sqrt(3) = signed magnitude of isotropic stress. These stress invariants are isomorphic to stress space in problems that involve no change in the orientation of the stress deviator. Thus, a plot of *r* vs. *z* is like a *q* vs. *p* plot (where *q* is von Mises equivalent stress and *p* is pressure) without geometrical distortion.

The yield gradient is

$$\frac{\partial f}{\partial \underset{\approx}{\sigma}} = \frac{\underset{\approx}{e}_r}{r_0} + \frac{\underset{\approx}{e}_z}{z_0} \tag{4.2}$$

Therefore, the unit normal to the yield surface is

$$\underset{\approx}{N} = \sin\phi\,\underset{\approx}{e}_z + \cos\phi\,\underset{\approx}{e}_r \tag{4.3}$$

Tensors $\mathbf{e}_z$ and $\mathbf{e}_r$ are respectively unit tensors in the directions of the identity tensor and the stress deviator.

where ϕ is the cone angle defined by $\tan\phi = r_0/z_0$. We will presume that the flow direction is of the same form but possibly using a different angle ψ. Therefore,

$$\underset{\approx}{P} = 3K(\sin\psi)\,\underset{\approx}{e}_z + 2G(\cos\psi)\,\underset{\approx}{e}_r \tag{4.4}$$

$$\underset{\approx}{Q} = 3K(\sin\phi)\,\underset{\approx}{e}_z + 2G(\cos\phi)\,\underset{\approx}{e}_r \tag{4.5}$$

Tensors P and Q are respectively the elastic stiffness operating on unit tensors **N** (normal to the yield surface) and **M** (in the flow direction).

The hydrostatic unit base tensor is simply the identity tensor divided by its own magnitude. Hence,

$$[\underset{\approx}{e}_z] = \frac{1}{\sqrt{3}}\begin{bmatrix} 1 & 0 & 0 \\ 0 & 1 & 0 \\ 0 & 0 & 1 \end{bmatrix} \tag{4.6}$$

For axisymmetric loading, the radial base tensor is

$$[\underset{\approx}{e}_r] = \frac{\pm 1}{\sqrt{6}}\begin{bmatrix} 2 & 0 & 0 \\ 0 & -1 & 0 \\ 0 & 0 & -1 \end{bmatrix} \tag{4.7}$$

Abbreviations TXE and TXC respectively denote triaxial extension and compression.

where positive is taken in TXE and negative applies in TXC. Hence,

$$P_A = \sqrt{3}K(\sin\psi) \pm \sqrt{\frac{2}{3}}2G(\cos\psi) \qquad P_L = \sqrt{3}K(\sin\psi) \mp \sqrt{\frac{2}{3}}G(\cos\psi) \tag{4.8}$$

For axisymmetric problems, subscripts "A" and "L" respectively stand for axial and lateral components of a tensor. Thus, these are components of the **P**-tensor (defined above).

$$Q_A = \sqrt{3}K(\sin\phi) \pm \sqrt{\frac{2}{3}}2G(\cos\phi) \qquad Q_L = \sqrt{3}K(\sin\phi) \mp \sqrt{\frac{2}{3}}G(\cos\phi) \tag{4.9}$$

and

$$\eta = 3K(\sin\psi)(\sin\phi) + 2G(\cos\psi)(\cos\phi) \tag{4.10}$$

Thus, the exact solutions for the axial and lateral stress rates are

$$\dot{\sigma}_A = \left[C - \frac{1}{\eta}P_A Q_A\right]\dot{\varepsilon}_A = \left[C - \frac{\left(\sqrt{3}K(\sin\psi) \pm \sqrt{\frac{2}{3}}2G(\cos\psi)\right)\left(\sqrt{3}K(\sin\phi) \pm \sqrt{\frac{2}{3}}2G(\cos\phi)\right)}{3K(\sin\psi)(\sin\phi) + 2G(\cos\psi)(\cos\phi)}\right]\dot{\varepsilon}_A$$

$$= \left[C - \frac{\left(3K^2(\sin\psi)(\sin\phi) + \frac{8}{3}G^2(\cos\psi)(\cos\phi) \pm \sqrt{2}4GK(\cos\psi)(\sin\phi)\right)}{3K(\sin\psi)(\sin\phi) + 2G(\cos\psi)(\cos\phi)}\right]\dot{\varepsilon}_A \tag{4.11a}$$

$$\dot{\sigma}_L = \left[\lambda - \frac{1}{\eta}P_L Q_A\right]\dot{\varepsilon}_A \tag{4.11b}$$

For piecewise linear strain histories, these can be integrated exactly to give piecewise linear stress histories.

Don't forget, this document is an excerpt from an unpublished working document, so this is a placeholder to refer to an analytical reduction of plasticity to axisymmetry.

Case: uniaxial stress. When the lateral stress is held constant, Eq. __ gives the solution for the lateral strain rate and axial stress rate

$$\dot{\varepsilon}_L = \left[\frac{\frac{1}{\eta}P_L Q_A - \lambda}{2\left(G + \lambda - \frac{1}{\eta}P_L Q_L\right)}\right]\dot{\varepsilon}_A \tag{4.12}$$

$$\dot{\sigma}_A = \left[2G + \lambda - \frac{1}{\eta}P_A Q_A\right]\dot{\varepsilon}_A + 2\left[\lambda - \frac{1}{\eta}P_A Q_L\right]\dot{\varepsilon}_L \tag{4.13}$$

EXAMPLE: Linear-elastic Linear Drucker-Prager yield with nonassociativity.

Table 4.1: Drucker-Prager parameters

Bulk modulus K	10000
Poisson's ratio ν	1/3
*Young's modulus K	10000
*shear modulus G	3750
*Lame modulus λ	7500
r_0	50
z_0	$50\sqrt{3}$
*yield normal $\underset{\sim}{N}$	$\frac{3\hat{\underset{\sim}{S}}+\underset{\sim}{I}}{2\sqrt{3}}$
flow direction $\underset{\sim}{M}$	$\frac{6\hat{\underset{\sim}{S}}+\underset{\sim}{I}}{\sqrt{39}}$

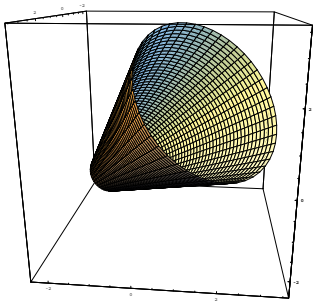

The physical units in Table 4.1 can be any self-consistent set of units. Incidentally, the strength was selected to be considerably smaller than the elastic moduli to ensure that strains would be small to help avoid issues associated with strain definitions. To replicate this analytical result, the stress definition must be work conjugate to the strain. Because this problem is of the fixed-axes type, the principal directions of the stretch and strain tensors are constant and therefore a logarithmic strain corresponds to Cauchy stress.

To assist researchers to independently reproduce our analytical solution, two yield functions corresponding to the above prescribed data are

$$f(r,z) = \frac{r}{r_0} + \frac{z}{z_0} - 1 = \frac{r}{50} + \frac{z}{50\sqrt{3}} - 1 \tag{4.14a}$$

$$f(I_1,J_2) = 3\sqrt{2J_2} + I_1 - 150\,, \tag{4.14b}$$

where

$$r = \sqrt{2J_2}\,, \qquad \text{and} \qquad z = I_1/\sqrt{3} \tag{4.15}$$

A flow potential whose gradient is parallel to the flow direction is

$$g(r,z) = \frac{r}{50} + \frac{z}{100\sqrt{3}} - 1 \tag{4.16a}$$

$$g(I_1,J_2) = 6\sqrt{2J_2} + I_1 - 300 \tag{4.16b}$$

Table 4.2: Piecewise linear axisymmetric driving strains

time	Axial strain, ε_A	Lateral strain, ε_L
0	0	0
1	$-\frac{17}{1800} = -0.00944444444444$	$-\frac{17}{1800} = -0.00944444444444$
2	$\frac{-(1+32\sqrt{6})}{1800} = -0.0441020398717$	$\frac{-1+16\sqrt{6}}{1800} = 0.0212176866025$
3	$\frac{11+16\sqrt{6}}{1800} = 0.0278843532692$	$\frac{11-8\sqrt{6}}{1800} = -0.00477550996793$
4	$\frac{645\sqrt{2}-1138\sqrt{3}}{9000(3\sqrt{2}+2\sqrt{3})} = -0.015266620380$	$\frac{-75\sqrt{2}+1598\sqrt{3}}{9000(3\sqrt{2}+2\sqrt{3})} = 0.0383755053393$

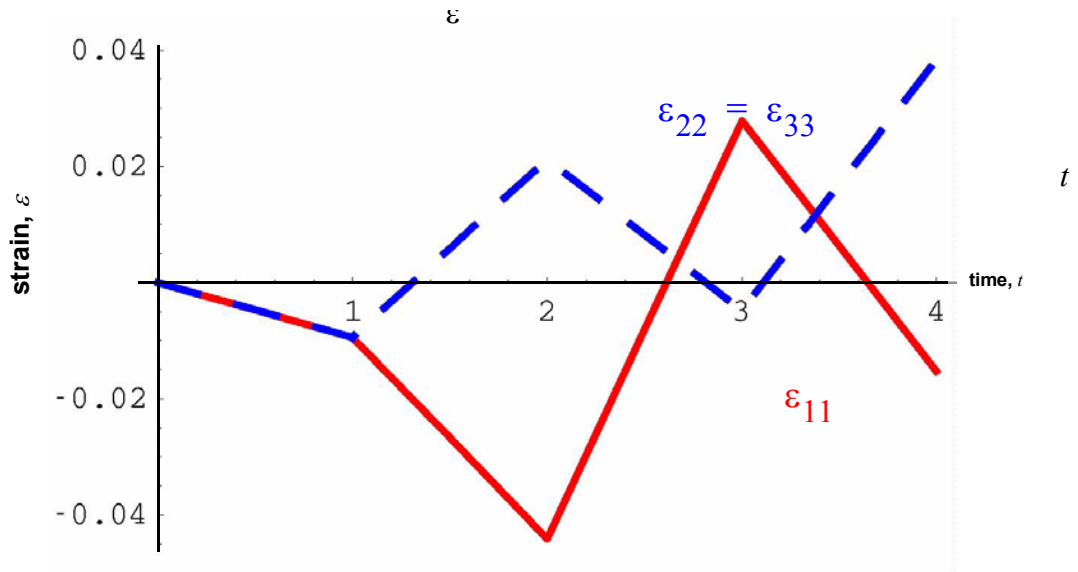

Figure 4.1. Driving strains for the Drucker-Prager verification test.

The driving strain path for this problem, given in Table 4.2 and Fig. 4.1, was devised so that the first two yield events would occur *exactly* halfway through the second and third leg. Moreover, this driving strain path was selected so that the trial elastic stress rate will be *exactly* parallel to the return projection direction in the second leg, and it will be *exactly* parallel to the yield surface normal in the third leg. The trial elastic stress rate for the final leg is slightly more shallow than the projection direction in the meridional plane.

At the time that this working document was written, the test code was not getting correct solutions at the vertex. This is evident in the errors at late time.

The exact solution is graphed in Fig. 4.2. The corresponding exact solutions for the Lode coordinates are shown in Fig. 4.10.

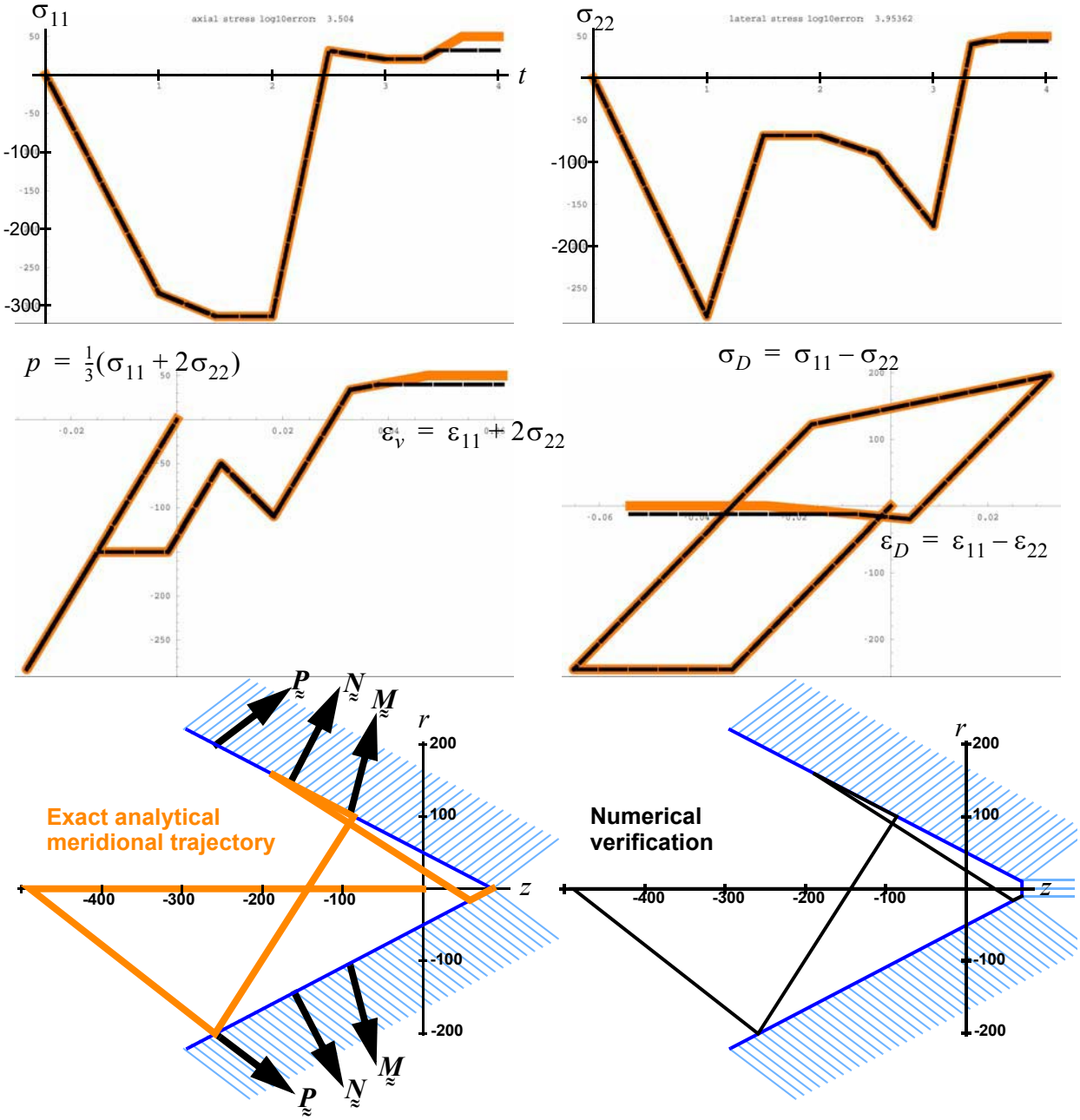

Figure 4.2. Exact solution corresponding to the driving strains prescribed in Table 4.2. The analytical results (thick orange lines) are shown along with a numerical simulation (thin black line) from the Sandia GeoModel [16], which supports Drucker-Prager yield functions except that its vertex is "clipped" as shown (therefore producing slight discrepancies in the results of the final leg). The Lode radius *r* in the meridional (*r* vs. *z*) plots is shown positive for TXE and negative for TXC.

This figure is a good case for using the isomorphic (Lode) stress invariants *r* and *z* instead of the more common *q* and *p*. With isomorphic invariants, the normal to the yield surface is actually normal to this 2D plot of *r* vs. *z* (such is not the case in a plot of *q* vs *p*)

The analytical solution of this problem must be broken into *at least* four separate legs because the prescribed strain path itself has four legs. However, some of these legs must be further broken into sub-legs where part of the interval is elastic and part is plastic. The exact solution is tabulated in Table 4.9. Each leg's name ends in E or P to indicate whether the leg (or sub-leg) is elastic or plastic. In the last sub-leg, the stress is stationary at the vertex while the strain continues to change.

Table 4.3: Exact Solution (axisymmetric Drucker-Prager non-associativity)

Leg	end time	reason for ending leg	ε_A	ε_L	σ_A	σ_L
1E	1	change in prescribed strain rate	$\frac{-17}{1800}$	$\frac{-17}{1800}$	$\frac{-850}{3}$	$\frac{-850}{3}$
2E	$\frac{3}{2}$	yield	$\frac{-9-16\sqrt{6}}{1800}$	$\frac{-9+8\sqrt{6}}{1800}$	$\frac{-50}{3}(9+4\sqrt{6})$	$\frac{50}{3}(2\sqrt{6}-9)$
2P	2	change in prescribed strain rate	$\frac{-1-32\sqrt{6}}{1800}$	$\frac{16\sqrt{6}-1}{1800}$	$\frac{-50}{3}(9+4\sqrt{6})$	$\frac{50}{3}(2\sqrt{6}-9)$
3E	$\frac{5}{2}$	yield	$\frac{5-8\sqrt{6}}{1800}$	$\frac{5+4\sqrt{6}}{1800}$	$\frac{50}{3}(2\sqrt{6}-3)$	$\frac{-50}{3}(3+\sqrt{6})$
3P	3	change in prescribed strain rate	$\frac{11+16\sqrt{6}}{1800}$	$\frac{11-8\sqrt{6}}{1800}$	$160\sqrt{\frac{2}{3}}-110$	$\frac{-10}{3}(33+8\sqrt{6})$
4E	$\frac{10}{3}$	yield	$\frac{645\sqrt{2}+14\sqrt{3}}{9000(3\sqrt{2}+2\sqrt{3})}$	$\frac{446\sqrt{3}-75\sqrt{2}}{9000(3\sqrt{2}+2\sqrt{3})}$	$160\sqrt{\frac{2}{3}}-110$	$10\left(\frac{58\sqrt{3}-49\sqrt{2}}{3\sqrt{2}+2\sqrt{3}}\right)$
4P	$\frac{5(7\sqrt{6}-22)}{12(\sqrt{6}-3)}$	vertex	$\frac{-89+32\sqrt{6}}{9000}$	$\frac{199+8\sqrt{6}}{9000}$	50	50
4V	4	end	$\frac{645\sqrt{2}-1138\sqrt{3}}{9000(3\sqrt{2}+2\sqrt{3})}$	$\frac{1598\sqrt{3}-75\sqrt{2}}{9000(3\sqrt{2}+2\sqrt{3})}$	50	50

**derived quantities*

This problem confirms that a non-associative plasticity model admits negative net work over a closed strain cycle. This problem was submitted as a letter to the editor of a highly ranked plasticity journal to disprove a contradictory claim (in paper that journal), which was based on an erroneous assertion that elastic strain increments can be assumed small compared to plastic strain increments. Rather than publishing our letter, the editor had the authors retract their incorrect work in one of their own later publications. The editor later chose not to publish yet another of our criticisms of those same authors even though the reviewers of our manuscript directly contradicted each other (one said that our claim couldn't possibly be right, while another asserted that our claims were well known to be true).

EXAMPLE: A loading path that includes a Sandler-Rubin closed strain cycle.

This example again uses a Linear Drucker-Prager yield criterion. In other words, the yield surface is a cone centered about the hydrostat so that the octahedral yield profile is a circle with Lode radius r that varies with pressure. The cone geometry is specified by the values of r_0 and z_0 cited in Table 4.1, where r_0 is the Lode radius at zero pressure and z_0 is the distance in stress space from the origin to the cone vertex. The tensor $\hat{\underset{\sim}{S}}$ that is used in Table 4.4 to define the yield normal and flow direction is the stress deviator, $\underset{\sim}{S}$, divided by its own magnitude (i.e., $\hat{\underset{\sim}{S}} \equiv \frac{\underset{\sim}{S}}{\sqrt{\underset{\sim}{S}:\underset{\sim}{S}}}$).

Table 4.4: Drucker-Prager parameters

Bulk modulus K	40000
Poisson's ratio ν	1/3
*Young's modulus E	40000
*shear modulus G	15000
*Lame modulus λ	30000
r_0	200
z_0	200
*yield normal $\underset{\sim}{N}$	$\dfrac{\hat{\underset{\sim}{S}} + \frac{\underset{\sim}{I}}{\sqrt{3}}}{\sqrt{2}}$
flow direction $\underset{\sim}{M}$	$\hat{\underset{\sim}{S}}$

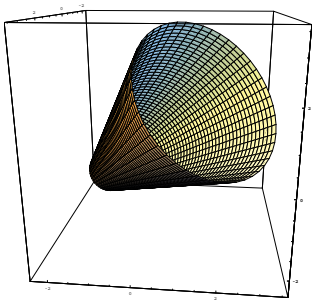

The parameters in Table 4.4 are in any self-consistent set of units. The strength was selected to be considerably smaller than the elastic moduli to ensure that strains would be small enough to avoid issues associated with strain definitions. To help researchers interpret and independently reproduce our analytical solution, two yield functions corresponding to the above prescribed data are

$$f(r,z) = \frac{r}{r_0} + \frac{z}{z_0} - 1 = \frac{r}{200} + \frac{z}{200} - 1 \qquad \text{where } r \equiv \sqrt{2J_2} \text{ and } z \equiv I_1/\sqrt{3} \qquad (4.17a)$$

$$f(I_1,J_2) = \sqrt{2J_2} + \frac{I_1}{\sqrt{3}} - 200\,, \qquad \text{where } J_2 \equiv \frac{1}{2}\underset{\sim}{S}:\underset{\sim}{S} \text{ and } I_1 = \operatorname{tr}\underset{\sim}{\sigma} \qquad (4.17b)$$

Two flow potentials whose gradients are parallel to the flow direction are

$$g(r,z) = \frac{r}{200} - 1 \qquad (4.18a)$$

$$g(I_1,J_2) = \sqrt{2J_2} - 200 \qquad (4.18b)$$

This material will be exercised under a piecewise linear strain history (which therefore has piecewise constant strain rates) that includes a closed strain cycle of the type discussed by Sandler, Rubin, and (later) Pucik. Specifically, the trial elastic stress rate during the interval $2 < t < 3$ points into the "Sandler-Rubin" wedge that is above the yield surface but below the flow potential. To make the cycle closed, the next leg has the same total strain rate except opposite in direction so that the strain at time $t = 4$ returns to the strain value at time $t = 2$.

Table 4.5: Piecewise linear axisymmetric driving strains

	time	Axial strain, ε_A	Lateral strain, ε_L
Leg 1: 0<*t*<1 hydrostatic	0	0	0
Leg 2: 1<*t*<2 shear up into yield	1	$\frac{-1}{200\sqrt{3}} = -0.00288675$	$\frac{-1}{200\sqrt{3}} = -0.00288675$
Leg 3: push into the Sandler-Rubin wedge	2	$-\left(\frac{3+32\sqrt{2}}{600\sqrt{3}}\right) = -0.0464332$	$\frac{16\sqrt{2}-3}{600\sqrt{3}} = 0.0188865$
	3	$\frac{6\sqrt{3}-11\sqrt{6}}{450} = 0.0367824$	$\frac{11\sqrt{2}-6}{300\sqrt{3}} = -0.0183912$
Leg 4: remove strain from the previous leg to close the cycle	4	$-\left(\frac{3+32\sqrt{2}}{600\sqrt{3}}\right) = -0.0464332$	$\frac{16\sqrt{2}-3}{600\sqrt{3}} = 0.0188865$

This is a Sandler-Rubin closed strain cycle

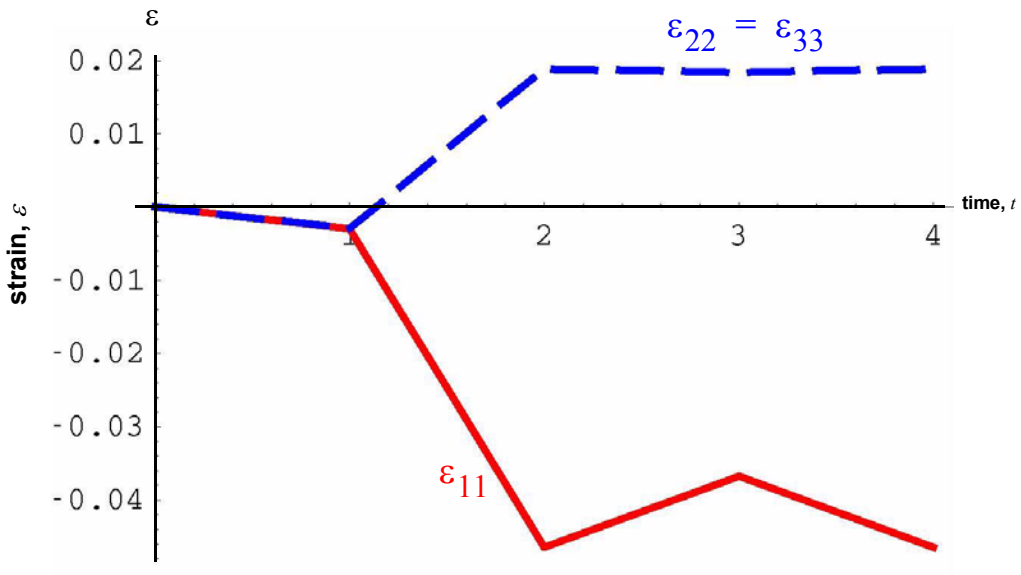

Figure 4.3. Driving strains for the Sandler-Rubin-Pucik verification test.

The driving strain path for this problem, which is given in Table 4.5 and Fig. 4.3, was devised so that the first yield event would occur *exactly* halfway through the second leg. The third leg, which begins and remains at yield, was designed so that the trial elastic stress rate would be parallel to $\underset{\approx}{N} - \underset{\approx}{M}$, thereby making the trial elastic stress rate have a positive inner product with the yield normal $\underset{\approx}{N}$ (which is a necessary condition for plastic flow), but a negative inner product with the flow direction $\underset{\approx}{M}$ (which is the situation studied by Sandler, Rubin, and Pucik). The magnitude of the strain rate during the third leg was selected such that the stress at the end of the leg would be purely deviatoric. The final leg, which is entirely elastic, was subjected to the same total strain increment in reverse so that the third and fourth legs together constitute a closed cycle in strain of the type considered by Sandler, Rubin, and Pucik.

The exact solution is graphed in Fig. 4.4, where the labels correspond to the exact solution at termination points of legs (or sublegs) as cited in the tabular exact solution in Table 4.6. For this problem, the Lode angle was always $+30°$ (i.e., triaxial compression).

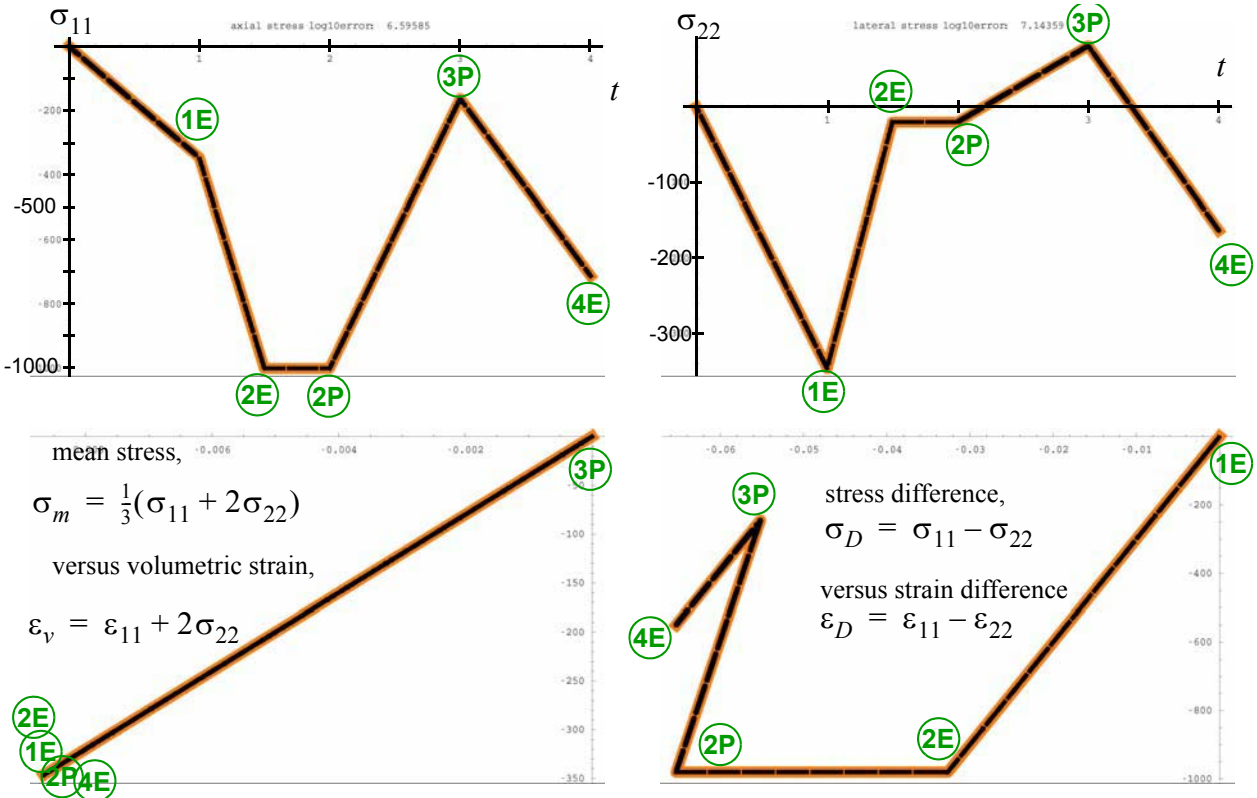

Figure 4.4. Exact solution corresponding to the driving strains prescribed in Table 4.5. The analytical results (thick orange lines) are shown along with a numerical simulation (thin black line) from the Sandia GeoModel [16]

The analytical solution of this problem must be broken into *at least* four separate legs because the prescribed strain path itself has four legs. However, leg 2 (spanning the time range $1 < t < 2$) must be further broken into sub-legs where part of the interval is elastic and part is plastic. The exact solution is tabulated in Table 4.6. Each leg's name ends in E or P to indicate whether the leg (or sub-leg) is elastic or plastic.

Table 4.6: Exact Solution (axisymmetric Sandler-Rubin type loading)

Leg	end time	reason for ending leg	ε_A	ε_L	σ_A	σ_L
1E	1	change in prescribed strain rate	$\frac{-1}{200\sqrt{3}}$	$\frac{-1}{200\sqrt{3}}$	$-200\sqrt{3}$	$-200\sqrt{3}$
2E	$\frac{3}{2}$	yield	$-\left(\frac{3+16\sqrt{2}}{600\sqrt{3}}\right)$	$\frac{8\sqrt{2}-3}{600\sqrt{3}}$	$\frac{-200(3+4\sqrt{2})}{\sqrt{3}}$	$\frac{200(2\sqrt{2}-3)}{\sqrt{3}}$
2P	2	change in prescribed strain rate	$-\left(\frac{3+32\sqrt{2}}{600\sqrt{3}}\right)$	$\frac{16\sqrt{2}-3}{600\sqrt{3}}$	$\frac{-200(3+4\sqrt{2})}{\sqrt{3}}$	$\frac{200(2\sqrt{2}-3)}{\sqrt{3}}$
3P	3	change in prescribed strain rate	$\frac{6\sqrt{3}-11\sqrt{6}}{450}$	$\frac{11\sqrt{2}-6}{300\sqrt{3}}$	$-200\sqrt{\frac{2}{3}}$	$100\sqrt{\frac{2}{3}}$
4E	4	end	$-\left(\frac{3+32\sqrt{2}}{600\sqrt{3}}\right)$	$\frac{16\sqrt{2}-3}{600\sqrt{3}}$	$\frac{200(2\sqrt{2}-9)}{\sqrt{3}}$	$-200\sqrt{\frac{2}{3}}$

The path through stress space for this problem is illustrated in Fig. 4.5, where we have multiplied the hydrostat axis by –1 to follow convention for predominantly compressive problems. The first leg is hydrostatic loading. Thereafter, the stress states are all triaxial compression. Leg 3 has a trial stress rate that forms a positive inner product with the yield normal but a negative inner product with the plastic flow direction, making it point into the "Sandler-Rubin wedge".

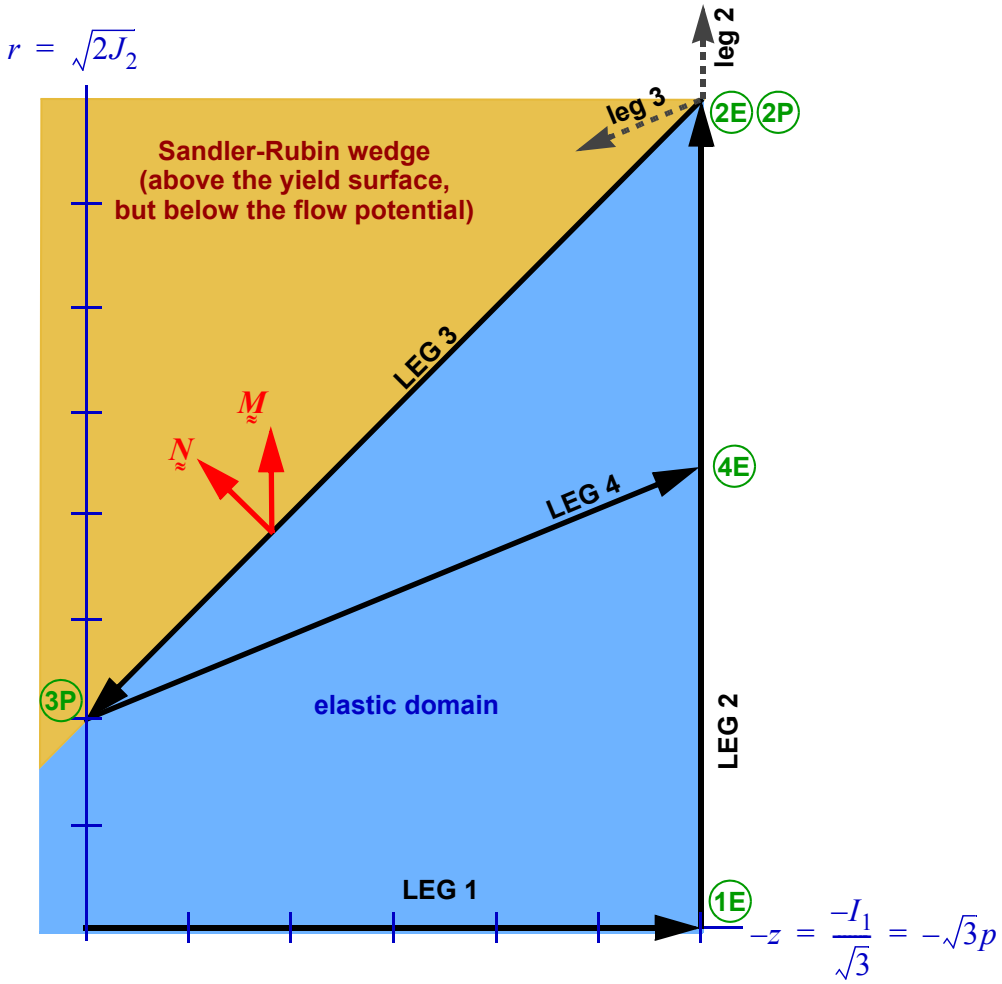

Figure 4.5. Meridional stress path. Dashed lines indicate the trial stress rate direction associated with the plastic legs. Note in particular, that leg 3 points into the Sandler-Rubin wedge.

Leg 3 and Leg 4 (spanning times from t=2 to t=4) are the primary area of interest for this verification problem. Because the total strain at time at t=4 is returned to its value at time t=2, the last two legs form a closed strain cycle of the type considered by Sandler and Rubin. Specifically, leg three (from t=2 to t=3) is plastic with the trial stress rate aligned with $\underset{\approx}{N} - \underset{\approx}{M}$, making it point above the yield surface but "below the flow potential" (i.e., $\dot{\underset{\approx}{\sigma}}^{\text{trial}} : \underset{\approx}{N} > 0$ but $\dot{\underset{\approx}{\sigma}}^{\text{trial}} : \underset{\approx}{M} < 0$).

Leg four (from t=3 to t=4) is elastic with a total strain increment equal in magnitude but opposite in direction to the strain increment of the preceding leg (i.e., it makes legs 3 and 4 together form a closed strain cycle). Sandler and Rubin presented an analysis "in the small" demonstrating that this type of closed strain cycle will have a negative total work over the cycle. Because our verification problem involves a yield normal and flow direction that is always constant, the tangent stiffness tensor is constant and the same for all plastic loading intervals. Hence, we may corroborate Sandler and Rubin's assertion "in the large" (i.e., for large strain increments).

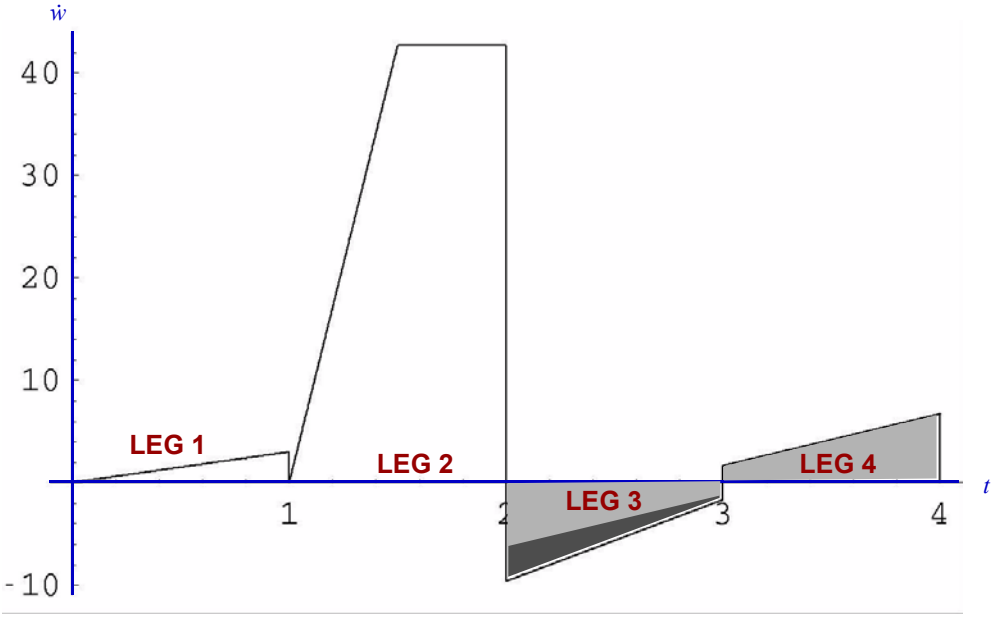

Figure 4.6. Work rate vs. time. The light shaded regions have identically equal area. The dark shaded region illustrates graphically the amount by which the work increments differ in the plastic and elastic parts of the Sandler-Rubin closed strain cycle formed by the last two load legs.

Figure 4.6 shows the work rate [namely $\dot{w} \equiv \underset{\sim}{\sigma} : \dot{\underset{\sim}{\varepsilon}} = \sigma_A \dot{\varepsilon}_A + 2(\sigma_L \dot{\varepsilon}_L)$]. As indicated in the figure, the total area under the work rate history for Legs 3 and 4 is negative, consistent with the assertions of Sandler and Rubin. The exact solution for the work increment during this closed strain cycle is

$$w|_2^4 \equiv \int_2^4 \dot{w} dt = 24 - 18\sqrt{2} = -1.45584 \qquad (4.19)$$

This confirms that this sample problem gives negative net work in a closed strain cycle.

Our plasticity code was verified to give the same result.

For more information about the fascinating fact that that any (classical) non-associative plasticity model can have a non-unique unstable release of energy, see the following publications:

1. Pučik, T., J.A. Burghardt, and R.M. Brannon (2015) Instability and nonuniqueness induced by nonassociated plastic flow -- Part 1: a case study, J. of the Mechanics of Materials and Structures, accepted May 2015.
2. Burghardt, J.A. and R.M. Brannon (2015) Instability and nonuniqueness induced by nonassociated plastic flow -- Part 2: investigation of three constitutive features that eliminate or delay the Sandler-Rubin instability, J. of the Mechanics of Materials and Structures, accepted May 2015.

As discussed by Sandler and Rubin, the possibility of negative work over a closed strain cycle does *not* violate the first or second laws of thermodynamics (i.e., it does not indicate the possibility of extracting unlimited energy by cycling through this total strain path). Repeating the strain cycle will produce entirely *elastic* response because, as seen in Fig. 4.5, state 4E (at the end of Leg 4) is different from state 2P (at the beginning of Leg 3). However, Sandler and Rubin do assert that the possibility of negative work in closed strain cycles implies non-uniqueness in dynamic problems that can lead to spontaneous motion from a quiescent state. This possibility was later verified numerically by Pucik, who showed that an infinitesimal strain pulse (namely one that leads to trial stress rates pointing into the Sandler-Rubin wedge) can grow in magnitude without bound.

Fixed-axes plane-stress Mohr-Coulomb plasticity

Analytical solutions are most tractable when the $\underset{\approx}{\boldsymbol{P}}$ and $\underset{\approx}{\boldsymbol{Q}}$ tensors are constant over extended time intervals. The Mohr-Coulomb yield criterion is a good choice for analytical solutions because (as illustrated in Fig. 4.7) its yield surface is piecewise planar, making its normal therefore constant over broad ranges of stresses on the yield surface.

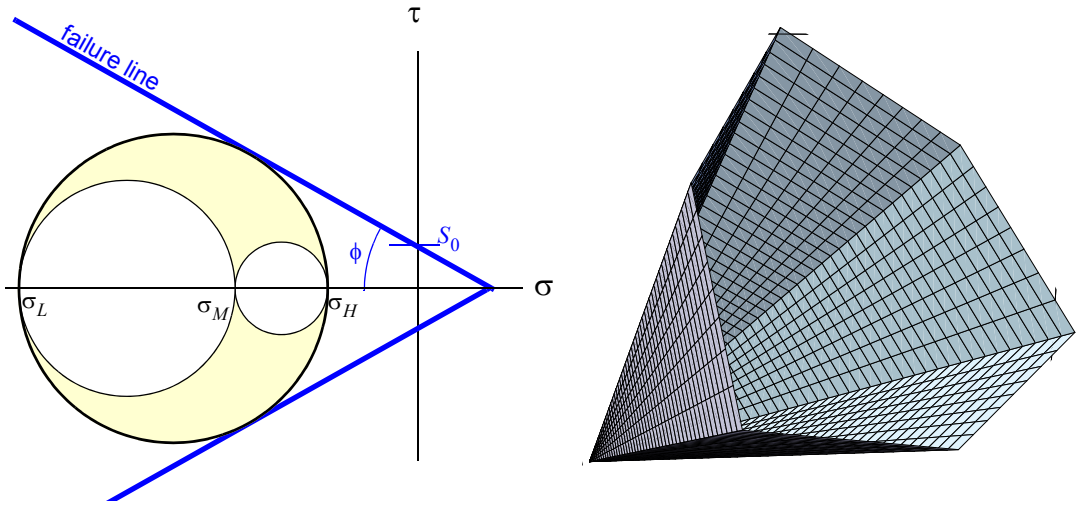

Figure 4.7. Mohr-Coulomb yield in the Mohr diagram and in stress space.

The Mohr-Coulomb yield criterion presumes yield occurs when the outer Mohr's circle in the Mohr diagram first touches a straight "failure line," as illustrated in Fig. 4.7. Working out the geometry of that figure shows that the Mohr-Coulomb failure criterion may be written

$$\frac{\sigma_H - \sigma_L}{2} = S_0 \cos\phi - \frac{\sigma_H + \sigma_L}{2}\sin\phi \tag{4.20}$$

Here, σ_L is the lowest principal stress and σ_H is the highest (we take stress positive in tension). The **friction angle** ϕ and the **cohesion** S_0 parameters quantify the slope and intercept of the failure line, as illustrated in Fig. 4.7.

A yield *function* corresponding to the yield *criterion* in Eq. 4.20 is

$$f = \frac{\sigma_H - \sigma_L}{2} - S_0 \cos\phi + \frac{\sigma_H + \sigma_L}{2}\sin\phi \tag{4.21}$$

The Mohr-Coulomb yield function is not differentiable at triaxial stress states (i.e., at states where the middle eigenvalue σ_M happens to equal the low or high eigenvalue). At non-triaxial states (where all three eigenvalues are distinct), the stress gradient of this yield function is

$$\underset{\approx}{\boldsymbol{B}} = \frac{\partial f}{\partial \underset{\approx}{\sigma}} = \frac{\partial f}{\partial \sigma_H}\underset{\approx}{\boldsymbol{e}}_H + \frac{\partial f}{\partial \sigma_L}\underset{\approx}{\boldsymbol{e}}_L = \frac{1}{2}(\sin\phi + 1)\underset{\approx}{\boldsymbol{e}}_H + \frac{1}{2}(\sin\phi - 1)\underset{\approx}{\boldsymbol{e}}_L \tag{4.22}$$

Here, $\underset{\approx}{\boldsymbol{e}}_H$ and $\underset{\approx}{\boldsymbol{e}}_L$ are eigenprojectors that indicate the location of the associated eigenvalue. For example, if the stress tensor is $[\underset{\approx}{\sigma}] = \text{DIAG}[\sigma_L, \sigma_M, \sigma_H]$, then $[\underset{\approx}{\boldsymbol{e}}_H] = \text{DIAG}[0, 0, 1]$ and $[\underset{\approx}{\boldsymbol{e}}_L] = \text{DIAG}[1, 0, 0]$. If, on the other hand, the eigenvalues are ordered differently such as $[\underset{\approx}{\sigma}] = \text{DIAG}[\sigma_M, \sigma_H, \sigma_L]$, then $[\underset{\approx}{\boldsymbol{e}}_H] = \text{DIAG}[0, 1, 0]$ and $[\underset{\approx}{\boldsymbol{e}}_L] = \text{DIAG}[0, 0, 1]$.

Because the eigenprojectors, $\underset{\approx}{\boldsymbol{e}}_H$ and $\underset{\approx}{\boldsymbol{e}}_L$, depend on the locations of the high and low eigenvalues, it is important to keep track of the eigenvalue ordering in analytical solutions. A change in the eigenvalue ordering during a loading leg will require splitting the leg into sub-legs to analyze each separately. A change in eigenvalue ordering, by the way, requires the stress state to pass through a triaxial condition where the yield function is non-differentiable because of yield surface vertices. To determine if vertex handling is necessary, you may obtain a stress solution based on the tentative assumption that only one of the planes is active (i.e., that the trial stress remains always *outside* the Koiter fan). If, after obtaining this tentative solution, the predicted stress is on or within the yield surface ($f = 0$) throughout the load interval, then the tentative single-surface solution was valid. Thankfully, our analysis will show that this particular verification problem requires no vertex handling because all changes in eigenvalue ordering occur only during *elastic* legs.

The yield function cited in Eq. 4.21 is not unique. For example, f^3 would be an equally acceptable yield function that satisfies sign conventions required for yield functions. Consequently, the yield gradient $\underset{\approx}{\boldsymbol{B}}$ in Eq. 4.22 is not unique. However, *the UNIT normal to the yield surface is unique.* Even though $\underset{\approx}{\boldsymbol{B}}$ depends on your choice of yield function, the unit tensor in the direction of $\underset{\approx}{\boldsymbol{B}}$ (evaluated on the yield surface) is the same for all choices of the yield function. The Mohr-Coulomb yield gradient in Eq. 4.22 was presented as a necessary first step to compute this unique *unit* normal to the yield surface:

$$\underset{\approx}{\boldsymbol{N}} = \frac{\underset{\approx}{\boldsymbol{B}}}{\|\underset{\approx}{\boldsymbol{B}}\|} = \frac{(\sin\phi + 1)\underset{\approx}{\boldsymbol{e}}_H + (\sin\phi - 1)\underset{\approx}{\boldsymbol{e}}_L}{\sqrt{2(\sin^2\phi + 1)}} \tag{4.23}$$

For linear-elastic non-hardening uncoupled plasticity, Eq. __ then gives

$$\underset{\approx}{\boldsymbol{Q}} = 2G\underset{\approx}{\boldsymbol{N}} + \lambda(\mathrm{tr}\underset{\approx}{\boldsymbol{N}})\underset{\approx}{\boldsymbol{I}}, \tag{4.24}$$

where

$$\mathrm{tr}\underset{\approx}{\boldsymbol{N}} = \frac{\sin\phi}{\sqrt{2(\sin^2\phi + 1)}} \qquad \text{and} \qquad \underset{\approx}{\boldsymbol{I}} = \mathrm{DIAG}[1, 1, 1] \tag{4.25}$$

Converting angles in the Mohr diagram to angles in stress space. The friction angle ϕ is the angle that the failure line makes with the σ-axis *in the Mohr diagram*. In *stress space*, however, the flat failure *planes* on the yield surface form a different angle Φ with the hydrostat given by

$$\sin\Phi = \underset{\approx}{\boldsymbol{N}} : \hat{\underset{\approx}{\boldsymbol{I}}} \tag{4.26}$$

Here, $\hat{\underset{\approx}{\boldsymbol{I}}}$ is a unit tensor in the direction of the identity tensor. Specifically, because the magnitude of the identity tensor is $\sqrt{3}$,

$$\hat{\underset{\approx}{\boldsymbol{I}}} = \underset{\approx}{\boldsymbol{I}}/\sqrt{3} \tag{4.27}$$

Therefore

$$\underset{\approx}{\boldsymbol{N}} : \hat{\underset{\approx}{\boldsymbol{I}}} = (\underset{\approx}{\boldsymbol{N}} : \underset{\approx}{\boldsymbol{I}})/\sqrt{3} = \mathrm{tr}\underset{\approx}{\boldsymbol{N}}/\sqrt{3} \tag{4.28}$$

Using Eq. 4.25 therefore allows the stress space friction angle Ψ to be related to the Mohr-space friction angle ψ by

$$\boxed{\sin\Phi = \underset{\approx}{N}:\hat{\underset{\approx}{I}} = \frac{\sin\phi}{\sqrt{6(\sin^2\phi + 1)}}} \qquad (4.29)$$

You can similarly define a stress-space *flow* angle Ψ by

$$\boxed{\sin\Psi = \underset{\approx}{M}:\hat{\underset{\approx}{I}} = \frac{\sin\psi}{\sqrt{6(\sin^2\psi + 1)}}} \qquad (4.30)$$

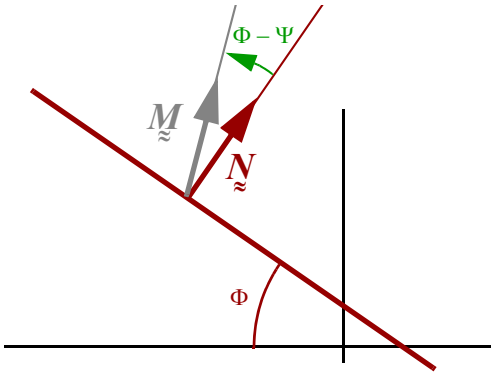

Figure 4.8. Meridional stress space.

We will soon solve a particular fixed-axis plane stress Mohr-Coulomb problem three different ways. In all three analyses, the material properties and the prescribed in-plane deformations will be identical and the *meridional* non-associativity will be identical. The solutions will dramatically differ, however, because three different flow rules will be used for the *deviatoric* non-associativity.

Flow direction for consistent nonassociativity. For consistent nonassociativity, the unit tensor $\underset{\approx}{M}$ in the direction of plastic flow is of the same form as Eq. 4.23 except with the friction angle ϕ replaced by the **dilatation angle** ψ :[1]

$$\underset{\approx}{M} = \frac{(\sin\psi + 1)\underset{\approx}{e}_H + (\sin\psi - 1)\underset{\approx}{e}_L}{\sqrt{2(\sin^2\psi + 1)}} \qquad (4.31)$$

Then Eq. __ gives

$$\underset{\approx}{P} = 2G\underset{\approx}{M} + \lambda(\mathrm{tr}\underset{\approx}{M})\underset{\approx}{I} \qquad (4.32)$$

where

$$\mathrm{tr}\underset{\approx}{M} = \frac{\sin\psi}{\sqrt{2(\sin^2\psi + 1)}} \qquad \text{and} \qquad \underset{\approx}{I} = \mathrm{DIAG}[1, 1, 1] \qquad (4.33)$$

Applying Eq. __ for linear elastic non-hardening ($H = 0$) uncoupled ($z_{ij} = 0$) plasticity gives the factor η needed to complete evaluation of the tangent stiffness tensor:

1. As seen in the upcoming example on page 64, this form for the plastic flow direction is fully non-associative. In the octahedral plane, it is not aligned with yield normal, nor is it radial.

$$\eta = M_{ij}E_{ijkl}N_{kl} = 2G\underset{\sim}{\boldsymbol{M}}:\underset{\sim}{\boldsymbol{N}} + \lambda(\mathrm{tr}\underset{\sim}{\boldsymbol{M}})(\mathrm{tr}\underset{\sim}{\boldsymbol{N}}) \tag{4.34}$$

where

$$\underset{\sim}{\boldsymbol{M}}:\underset{\sim}{\boldsymbol{N}} = \frac{(\sin\psi)(\sin\phi)+1}{\sqrt{(\sin^2\psi+1)(\sin^2\phi+1)}}. \tag{4.35}$$

These may be used in Eq. 2.39 to obtain the out-of-plane strain rate $\dot{\varepsilon}_3$, which may then be used in Eqs. 2.25a and 2.25b to obtain the in-plane stresses for problems that are driven by prescribed in-plane strains. Of course, during elastic legs, terms involving $\underset{\sim}{\boldsymbol{P}}$ and $\underset{\sim}{\boldsymbol{Q}}$ are merely omitted.

Consistent non-normality computes the yield normal and flow directions by algebraically identical formulas:

$$\underset{\sim}{\boldsymbol{N}} = \frac{(\sin\phi+1)\underset{\sim}{\boldsymbol{e}}_H + (\sin\phi-1)\underset{\sim}{\boldsymbol{e}}_L}{\sqrt{2(\sin^2\phi+1)}} \text{ and } \underset{\sim}{\boldsymbol{M}} = \frac{(\sin\psi+1)\underset{\sim}{\boldsymbol{e}}_H + (\sin\psi-1)\underset{\sim}{\boldsymbol{e}}_L}{\sqrt{2(\sin^2\psi+1)}}. \tag{4.36}$$

The *stress-space* friction and dilatation angles,

$$\sin\Phi = \frac{\sin\phi}{\sqrt{6(\sin^2\phi+1)}} \text{ and } \sin\Psi = \frac{\sin\psi}{\sqrt{6(\sin^2\psi+1)}}, \tag{4.37}$$

allow the consistent normal and flow tensors to be written as

$$\underset{\sim}{\boldsymbol{N}} = \cos\Phi\underset{\sim}{\nu} + \sin\Phi\hat{\underset{\sim}{\boldsymbol{I}}} \text{ and } \underset{\sim}{\boldsymbol{M}} = \cos\Psi\underset{\sim}{\mu} + \sin\Psi\hat{\underset{\sim}{\boldsymbol{I}}} \tag{4.38}$$

where

$$\underset{\sim}{\nu} = \frac{\underset{\sim}{\boldsymbol{N}}^d}{\left\|\underset{\sim}{\boldsymbol{N}}^d\right\|} \text{ and } \underset{\sim}{\mu} = \frac{\underset{\sim}{\boldsymbol{M}}^d}{\left\|\underset{\sim}{\boldsymbol{M}}^d\right\|} \tag{4.39}$$

Here, the superscript d denotes the "deviatoric part." For consistent non-associativity the unit tensors $\underset{\sim}{\nu}$ and $\underset{\sim}{\mu}$ *are not equal* — they are computed in manners consistent with the meaning of the friction angle and dilatation angle, respectively.

Comparing the left and right sides of the above four equations shows that consistent non-associativity uses the friction and dilatation angles in *algebraically identical ways*. For consistent non-normality, the flow direction has a component perpendicular to the plane spanned by the yield normal and the hydrostat, making $\underset{\sim}{\mu} \neq \underset{\sim}{\nu}$.

Flow direction for deviatoric associativity. The term "deviatoric associativity" means that the flow tensor $\underset{\sim}{\boldsymbol{M}}$ and the yield normal $\underset{\sim}{\boldsymbol{N}}$ are nonparallel in the meridional plane, but they are parallel in the octahedral plane. Hence, the flow tensor $\underset{\sim}{\boldsymbol{M}}$ and the yield normal $\underset{\sim}{\boldsymbol{N}}$ have parallel *deviatoric* parts. For deviatoric associativity, the unit tensor $\underset{\approx}{\mu}$ in Eq. 4.38 is replaced by the unit tensor $\underset{\approx}{\nu}$ from the *yield* normal in Eq. 4.38 so that

$$\underset{\sim}{\boldsymbol{M}} = \cos\Psi \underset{\approx}{\nu} + \sin\Psi \hat{\underset{\sim}{\boldsymbol{I}}} \tag{4.40}$$

This flow direction may be expressed directly in terms of the yield normal as

$$\underset{\sim}{\boldsymbol{M}} = \frac{\cos\Psi}{\cos\Phi}[\underset{\sim}{\boldsymbol{N}} - \sin\Phi \hat{\underset{\sim}{\boldsymbol{I}}}] + \sin\Psi \hat{\underset{\sim}{\boldsymbol{I}}} \tag{4.41}$$

This flow direction still forms the same angle with the hydrostat as it did in the fully non-associative case (Fig. 4.8), but it is associative in the octahedral plane. The deviatoric parts of $\underset{\sim}{\boldsymbol{M}}$ and $\underset{\sim}{\boldsymbol{N}}$ are not *equal* — they are simply *parallel*.

As with full associativity, the projection direction $\underset{\sim}{\boldsymbol{P}}$ tensor is still computed using Eq. __

$$\underset{\sim}{\boldsymbol{P}} = 2G\underset{\sim}{\boldsymbol{M}} + \lambda(\mathrm{tr}\underset{\sim}{\boldsymbol{M}})\underset{\sim}{\boldsymbol{I}} \tag{4.42}$$

and the η factor that appears in the tangent stiffness is still given by

$$\eta = M_{ij}E_{ijkl}N_{kl} = 2G\underset{\sim}{\boldsymbol{M}}:\underset{\sim}{\boldsymbol{N}} + \lambda(\mathrm{tr}\underset{\sim}{\boldsymbol{M}})(\mathrm{tr}\underset{\sim}{\boldsymbol{N}}) \tag{4.43}$$

The trace of the flow direction for deviatoric associativity is identical to what it was for consistent non-associativity. Namely,

$$\mathrm{tr}\underset{\sim}{\boldsymbol{M}} = \frac{\sin\psi}{\sqrt{2(\sin^2\psi + 1)}} \tag{4.44}$$

Deviatoric associativity alters $\underset{\sim}{\boldsymbol{P}}$ by changing its deviatoric part, and it alters η by changing the angle between $\underset{\sim}{\boldsymbol{M}}$ and $\underset{\sim}{\boldsymbol{N}}$, which is quantified by $\underset{\sim}{\boldsymbol{M}}:\underset{\sim}{\boldsymbol{N}}$.

Flow direction for Drucker-Prager non-normality. Whereas deviatoric associativity corresponds to replacing the deviatoric flow direction $\underset{\approx}{\mu}$ in Eq. 4.38 with the deviatoric yield direction $\underset{\approx}{\nu}$, Drucker-Prager non-normality replaces $\underset{\approx}{\mu}$ with a unit tensor in the direction of the stress deviator. With consistent and deviatoric non-normality, a Mohr-Coulomb model retains the property that large expanses of stress space have constant yield normals and flow directions, which greatly simplifies analytical solutions. With Drucker-Prager non-normality, this attractive

feature is lost, but it is nonetheless an important flow model to consider because many numerical plasticity codes return the stress to the yield surface in such a way that the updated stress deviator points in the same direction as the trial stress deviator, which (for linear elasticity) implies a Drucker-Prager flow rule.

EXAMPLE 1 (consistent non-associativity)

Here we consider a Mohr-Coulomb elastoplasticity problem for which the in-plane strains are prescribed as functions of time. The out-of-plane strain, as well as the in-plane stresses, are desired. Let the in-plane strains be piecewise linear as defined in Table 4.7. The material parameters are listed in Table 4.7.

Table 4.7: Piecewise linear strain path

time	ε_{11}	ε_{22}
0	0	0
0.1	-0.8×10^{-3}	-0.8×10^{-3}
0.2	0.3×10^{-3}	-1.2×10^{-3}
0.3	0.3×10^{-3}	-4.0×10^{-3}
0.4	-1.0×10^{-3}	-3.5×10^{-3}
0.5	-4.9×10^{-3}	-2.0×10^{-3}
0.6	-3.9×10^{-3}	-4.0×10^{-3}
0.7	-3.9×10^{-3}	-2.0×10^{-3}

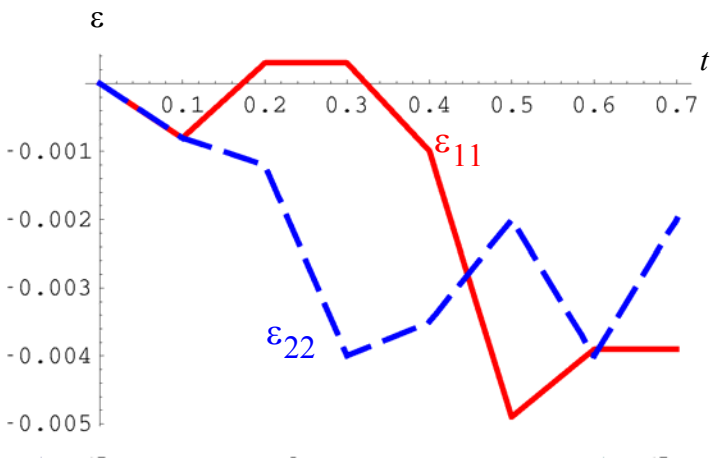

Table 4.8: Mohr-Coulomb material parameters (SI units)

Young's modulus E	31000
Poisson's ratio ν	0.26
*bulk modulus K	21527.78
*shear modulus G	12301.59
*Lame constant λ	13326.72
Cohesion S_0	15.7
friction angle ϕ	29°
dilatation angle ψ	14°

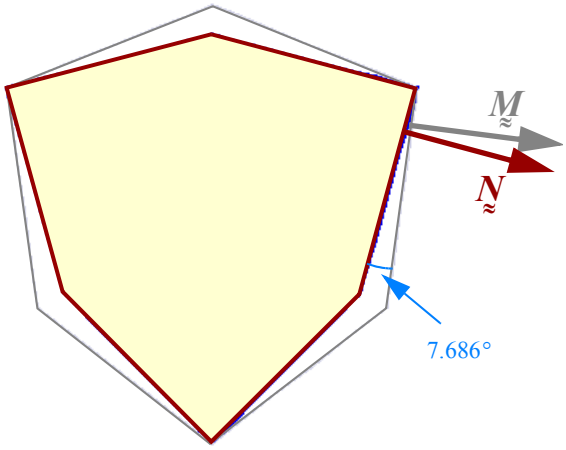

To assist researchers to independently reproduce our analytical solution, two yield functions[1] corresponding to the above prescribed data are

$$f(\sigma_L, \sigma_H) = (1.02249)\sigma_H - (0.354779)\sigma_L - 18.9121 \tag{4.45a}$$

$$f(r, \theta, z) = r[(0.973878)\cos\theta + (0.272593)\sin\theta] + (0.385505)z - 18.9121\,, \tag{4.45b}$$

where

$$r = \sqrt{2J_2}\,, \qquad \theta = \frac{1}{3}\text{ArcSin}\left[\frac{J_3}{2}\left(\frac{3}{J_2}\right)^{3/2}\right], \qquad z = I_1/\sqrt{3} \tag{4.46}$$

1. Yield functions are not unique. This particular yield function is defined so that the coefficient of r will evaluate to 1.0 in triaxial compression $(\theta = -\pi/6)$. Eq. 4.45 represents *the same function* expressed in terms of principal stresses and in terms of cylindrical Lode coordinates.

A flow potential whose gradient is parallel to the flow direction is

$$g(\sigma_L, \sigma_H) = (0.779917)\sigma_H - (0.476067)\sigma_L \tag{4.47a}$$

$$g(r, \theta, z) = r[(0.888115)\cos\theta + (0.124046)\sin\theta] + (0.175428)z\,, \tag{4.47b}$$

The exact solution is graphed in Fig. 4.9. The corresponding exact solutions for the Lode coordinates are shown in Fig. 4.10.

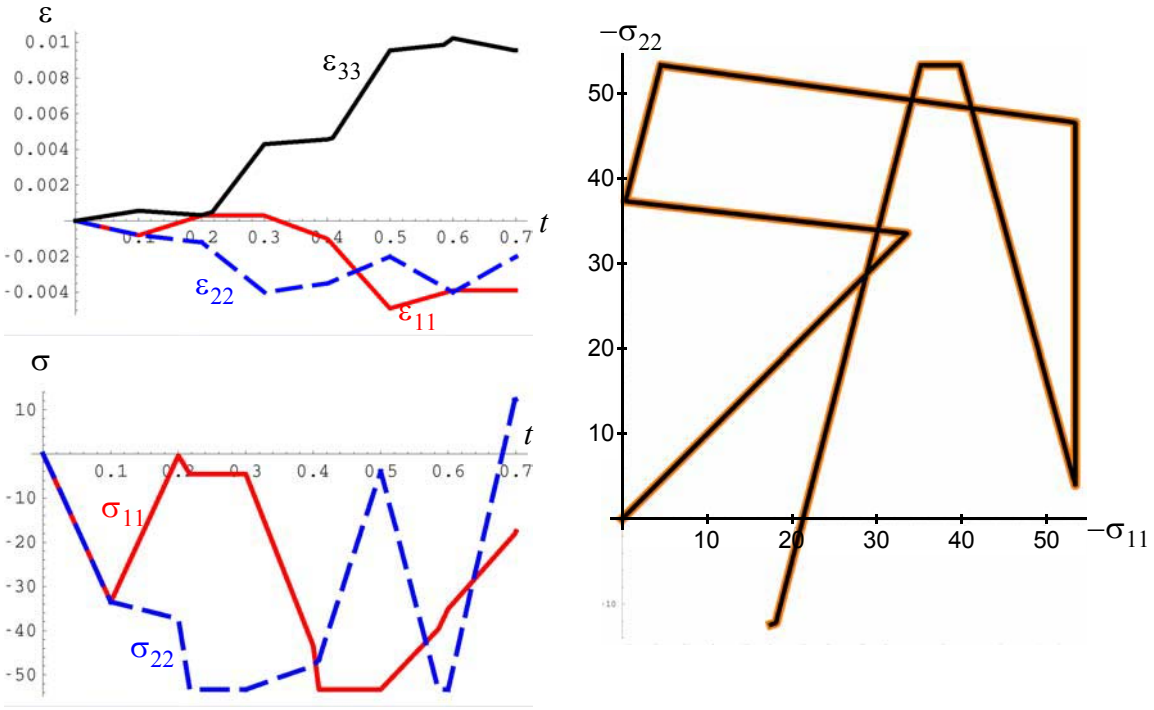

Figure 4.9. Exact plane stress solution for the in-plane stress history and out-of-plane strain history corresponding to the in-plane driving strains prescribed in Table 4.7. The stress diagram shows the analytical solution (thick orange line) overlaid with a numerical solution (thin black line) from the Sandia GeoModel [16].

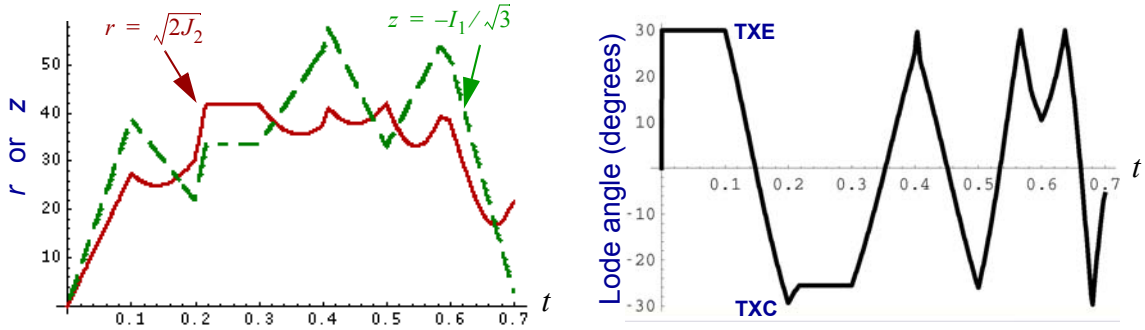

Figure 4.10. Exact solution for Lode coordinates. In this manuscript, the Lode angle is defined to be positive in triaxial extension (TXE) and negative in triaxial compression (TXC).

The analytical solution of this problem must be broken into *at least* seven separate legs because the prescribed strain path itself has seven legs. However, some of these legs must be further broken into sub-legs where part of the interval is elastic and part is plastic. The exact solution is tabulated in Table 4.9. Each leg's name ends in E or P to indicate whether the leg (or sub-leg) is elastic or plastic.

Table 4.9: Exact Solution (consistent non-associativity)

Leg	end time	reason for ending leg	ε_{11} (10^{-3}) at end	ε_{22} (10^{-3}) at end	ε_{33} (10^{-3}) at end	σ_{11} at end	σ_{33} at end
1E (LLH)	0.1	change in prescribed strain rate	–0.8	–0.8	0.56216	–33.5135	–33.5135
2E (MLH)	0.2	change in prescribed strain rate	0.3	–1.2	0.31622	–0.39897	–37.3037
3E (MLH)	0.21719	yield	0.3	–1.68133	0.48533	–4.55972	–53.3066
3P (MLH)	0.3	change in prescribed strain rate	0.3	–4.0	4.2839	–4.55972	–53.3066
4E (MLH)	0.4	change in prescribed strain rate	–1.0	–3.5	4.56500	–43.4593	–47.9205
5E (MLH) (LMH)	0.408438	yield	–1.32909	–3.37343	4.63614	–53.3066	–46.5770
5P (LMH)	0.5	change in prescribed strain rate	–4.9	–2.0	9.54409	–53.3066	–3.9808
6E (LMH) (MLH)	0.585264	yield	–4.04736	–3.70528	9.84366	–39.6995	–53.3066
6P (MLH)	0.6	change in prescribed strain rate	–3.9	–4.0	10.2254	–35.1313	–53.3066
7E (MLH) (LMH) (LHM)	0.69854	yield	–3.9	–2.0292	9.53297	–18.0951	12.2175
7P (LHM)	0.7	change in prescribed strain rate	–3.9	–2.0	9.52648	–17.5211	12.4166

The eigenvalue ordering during each leg is shown in the first column. For example, the ordering MLH indicates that σ_{11}, σ_{22}, and σ_{33} are the middle, low, and high eigenvalues respectively. In leg 5E, the ordering of stress eigenvalues for the elastic solution is initially MLH, but changes to LMH. Determining if a trial elastic solution is valid requires carefully monitoring eigenvalue ordering. In this consistent associativity problem, the stresses fortuitously don't change ordering during plastic legs, happily avoiding the need for vertex analysis.

A scaled meridional stress path is shown in Fig. 4.11. The stress moves through a full range of Lode angles in this problem. To compensate for the fact that meridional profiles of the yield surface are different at different Lode angles, Fig. 4.11 scales the ordinate so that the local meridional limit coincides with the TXC profile. By using this scaling, motion of the stress relative to the yield surface is more readily apparent.

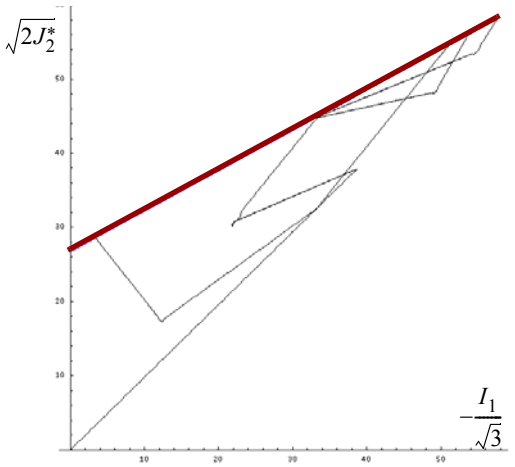

Figure 4.11. Trajectory in stress space. The vertical axis of this meridional profile is scaled to place the local meridional profile (which varies with Lode angle) coincident with the TXC profile.

Table 4.10: Normal and flow directions

Leg	$\underset{\sim}{N}$	$\underset{\sim}{M}$
3P (MLH)	DIAG[0, N_L, N_H]	DIAG[0, M_L, M_H]
5P (LMH)	DIAG[N_L, 0, N_H]	DIAG[M_L, 0, M_H]
6P (MLH)	DIAG[0, N_L, N_H]	DIAG[0, M_L, M_H]
7P (LHM)	DIAG[N_L, N_H, 0]	DIAG[M_L, M_H, 0]

For each plastic leg, $\eta = 26775.7$, and Table 4.10 shows the unit normal to the yield surface $\underset{\sim}{N}$, the unit tensor $\underset{\sim}{M}$ in the direction of plastic flow, where $N_L = -0.3278$, $N_H = 0.9447$, $M_L = -0.521$, and $M_H = 0.8535$. The yield normal $\underset{\sim}{N}$ and flow direction $\underset{\sim}{M}$ point in different directions on the meridional plane (specifically the trace of $\underset{\sim}{M}$ is smaller than the trace of $\underset{\sim}{N}$). For consistent non-associativity, the $\underset{\sim}{N}$ and $\underset{\sim}{M}$ tensors are *also* misaligned in the octahedral plane, as indicated on page 64. To match this analytical solution, *numerical schemes must use the consistent flow direction.* After showing a few of the actual computations associated with Leg 5P of this example, we will solve this same problem using two other flow rules that have the same non-normality on the meridional plane, but different non-normality on the octahedral plane. Computations associated with the other plastic legs are similar.

Detailed analysis of leg 5P. To illustrate how the normal and flow directions in this exact solution were determined (and then used to update stress and strain), we will consider Leg 5P. Analysis of the elastic legs is conventional, and therefore will not be discussed. All of the plastic legs are similar to Leg 5, so only this leg will be explained.[1] Leg 5 begins elastic, but ends plastic. The elastic solution applies until the yield criterion is reached at time $t^{\text{yield}} = 0.408438$. The stress and strain tensors (determined from integration of the elasticity equations from $t = 0.4$ to $t = 0.408438$) at the onset of yield were found to be

$$\text{At } t^{\text{yield}} = 0.408438,$$

$$\underset{\approx}{\sigma}^{\text{yield}} = \text{DIAG}[-53.3066, -46.557, 0] \tag{4.48a}$$

$$\underset{\approx}{\varepsilon}^{\text{yield}} = \text{DIAG}[-0.001329, -0.003373, 0.004636] \tag{4.48b}$$

These serve as the initial conditions needed to integrate Eq. 2.25 through Leg 5P. The lion's share of the work is, of course, determining the tangent components of the $\underset{\approx}{\boldsymbol{P}}$ and $\underset{\approx}{\boldsymbol{Q}}$ tensors that appear in Eq. 2.25.

Equation 4.48a shows that the numerically smallest principal stress at time t^{yield} is located in the first position, whereas the largest principal stress is in the 3rd position. The eigenprojectors are diagonal tensors with a 1 marking the location of the associated eigenvalue:

$$\underset{\approx}{\boldsymbol{e}}_L = \text{DIAG}[1, 0, 0] \quad \text{and} \quad \underset{\approx}{\boldsymbol{e}}_H = \text{DIAG}[0, 0, 1] \tag{4.49}$$

The plastic part of leg 5 is solved by tentatively presuming that this eigenvalue ordering will be preserved throughout the remainder of the leg. When the solution is complete, this assumption will be shown to be satisfied. The projectors in Eq. 4.49 are substituted into the formulas for the yield normal and flow direction (Eqs. 4.23 and 4.31) to obtain

$$\underset{\sim}{\boldsymbol{N}} = \frac{(\sin 29^\circ + 1)\boldsymbol{DIAG}[0, 0, 1] + (\sin 29^\circ - 1)\boldsymbol{DIAG}[1, 0, 0]}{\sqrt{2(\sin^2 29^\circ + 1)}} = \text{DIAG}[-0.327802,\ 0\ , 0.944746] \tag{4.50}$$

$$\underset{\sim}{\boldsymbol{M}} = \frac{(\sin 14^\circ + 1)\boldsymbol{DIAG}[0, 0, 1] + (\sin 14^\circ - 1)\boldsymbol{DIAG}[1, 0, 0]}{\sqrt{2(\sin^2 14^\circ + 1)}} = \text{DIAG}[-0.521013,\ 0\ , 0.853549] \tag{4.51}$$

The scalar η is computed by using Eq. 4.34 via the following sequence of calculations:

$$\underset{\sim}{\boldsymbol{M}}:\underset{\sim}{\boldsymbol{N}} = \frac{(\sin\psi)(\sin\phi) + 1}{\sqrt{(\sin^2\psi + 1)(\sin^2\phi + 1)}} = \frac{(\sin 14^\circ)(\sin 29^\circ) + 1}{\sqrt{(\sin^2 14^\circ + 1)(\sin^2 29^\circ + 1)}} = 0.97718\,. \tag{4.52}$$

---

1. A *Mathematica* notebook that contains all of the necessary calculations is available upon request.

$$\mathrm{tr}\underset{\sim}{N} = \frac{2\sin 29^\circ}{\sqrt{2(\sin^2 29^\circ + 1)}} = 0.30847 \tag{4.53}$$

$$\mathrm{tr}\underset{\sim}{M} = \frac{2\sin 14^\circ}{\sqrt{2(\sin^2 14^\circ + 1)}} = 0.66507 \tag{4.54}$$

$$\eta = 2G(\underset{\sim}{M}:\underset{\sim}{N}) + \lambda(\mathrm{tr}\underset{\sim}{M})(\mathrm{tr}\underset{\sim}{N})$$

$$= 2(12301.59)(0.97718) + (13326.72)(0.66507)(0.30847)$$

$$= 26775.7 \tag{4.55}$$

Applying Eqs. 4.24 and 4.32 gives

$$\underset{\approx}{Q} = 2G\,\underset{\sim}{N} + \lambda(\mathrm{tr}\underset{\sim}{N})\,\underset{\approx}{I}$$

$$= 2(12301.59)\,\mathbf{DIAG}[-0.327802,\ 0,\ 0.944746] + (13326.72)(0.30847)\,\mathbf{DIAG}[1,\ 1,\ 1]$$

$$= \mathrm{DIAG}[156.856,\ 8221.84,\ 31465.6] \tag{4.56}$$

$$\underset{\approx}{P} = 2G\,\underset{\sim}{M} + \lambda(\mathrm{tr}\underset{\sim}{M})\,\underset{\approx}{I}$$

$$= 2(12301.59)\ \mathbf{DIAG}[-0.521013,\ 0\ ,\ 0.853549] + (13326.72)(0.66507)\ \mathbf{DIAG}[1,\ 1,\ 1]$$

$$= \mathrm{DIAG}[-8386.94,\ \ 4431.62\ ,\ 25431.6] \tag{4.57}$$

The prescribed (in-plane) strains are piecewise linear functions of time. Therefore, the strain *rate* is piecewise constant. During Leg 5, Table 4.7 implies that the in-plane strain rates are

$$\dot{\varepsilon}_{11} = \frac{(-4.9\times 10^{-3}) - (-1.0\times 10^{-3})}{0.5 - 0.4} = -0.039 \tag{4.58}$$

$$\dot{\varepsilon}_{22} = \frac{(-2.0\times 10^{-3}) - (-3.5\times 10^{-3})}{0.5 - 0.4} = 0.015 \tag{4.59}$$

Using Eq. 2.39, the rate of out-of-plane strain is therefore given by

$$\dot{\varepsilon}_{33} = \frac{\lambda(\dot{\varepsilon}_{11} + \dot{\varepsilon}_{22}) - \frac{1}{\eta}P_{33}[Q_{11}\dot{\varepsilon}_{11} + Q_{22}\dot{\varepsilon}_{22}]}{\frac{1}{\eta}P_{33}Q_{33} - [2G + \lambda]}$$

$$= \frac{(13326.7)(-0.039 + 0.015) - \frac{1}{26775.7}(25431.6)[156.856(-0.039) + (8221.84)(0.015)]}{\frac{1}{26775.7}(25431.6)(31465.6) - [2(12301.59) + (13326.7)]}$$

$$= 0.0536026 \tag{4.60}$$

Hence, the strain rate tensor during Leg 5P (i.e., $0.408438 < t < 0.5$) is

$$\dot{\underset{\sim}{\varepsilon}} = \text{DIAG}[\,-0.039\,,\ 0.015\,,\ 0.0536026\,] \tag{4.61}$$

This strain rate is *constant* for because the in-plane strain rates are both constant throughout leg 5 and because the $\underset{\sim}{\boldsymbol{P}}$ and $\underset{\sim}{\boldsymbol{Q}}$ tensors themselves will remain constant as long as the stress eigenvalue ordering is preserved. The domain of validity of Eq. 4.60 would end if a triaxial state develops before the end of Leg 5, but we will show that no eigenvalue re-ordering occurs on the interval $0.408438 < t < 0.5$. Hence the constant strain rate in Eq. 4.61 applies through the end of Leg 5.

The out-of-plane stress rate is, by design, zero. The constant in-plane stress rates during this interval are obtained by substituting Eq. 4.60 into 2.25a and 2.25b to give

$$\dot{\underset{\sim}{\sigma}} = \text{DIAG}[\ 0\ ,\ 465.0\ ,\ 0\ ] \tag{4.62}$$

Hence, the linear time-varying stress and strains after yield are

$$\underset{\sim}{\varepsilon} = \underset{\sim}{\varepsilon}^{\text{yield}} + \dot{\underset{\sim}{\varepsilon}}(t - t^{\text{yield}}) \tag{4.63}$$

$$\underset{\sim}{\sigma} = \underset{\sim}{\sigma}^{\text{yield}} + \dot{\underset{\sim}{\sigma}}(t - t^{\text{yield}}) \tag{4.64}$$

where the initial states, $\underset{\sim}{\varepsilon}^{\text{yield}}$ and $\underset{\sim}{\sigma}^{\text{yield}}$ are specified in Eq. 4.48. The eigenvalue ordering associated with this solution remains unchanged throughout the interval from $0.408438 < t < 0.5$. Consequently, it is valid through the end of Leg 5.

EXAMPLE 2 (deviatoric associativity)

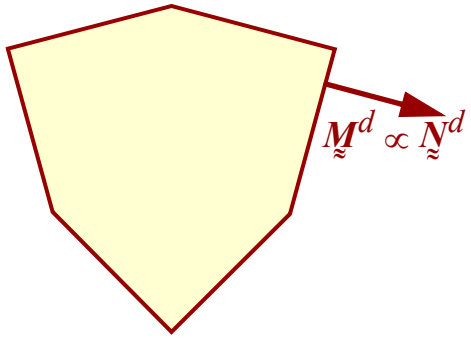

Here we consider the same Mohr-Coulomb elastoplasticity problem, but this time the flow rule is replaced by deviatoric associativity. The in-plane strains and material parameters are identical to those defined in Tables 4.7. and 4.8.

For deviatoric associativity, the dilatation angle ψ from Table 4.8 is used in Eq. 4.30 to compute a stress-space angle Ψ that is identical to the stress-space angle for consistent non-associativity. Consistent non-associativity applies Eq. 4.38 to compute the flow direction, but deviatoric associativity uses Eq. 4.40, which makes the *deviatoric parts* of the flow direction and yield normal parallel. The angle between the flow direction and the hydrostat remains as it was in the consistent non-associativity case. Other than this, the yield models are identical. As we will soon see, this small change leads to dramatic differences in the stress response.

The *yield function* corresponding to the material data in Tables 4.7 is identical to what it was in the consistent non-associativity problem:

$$f(\sigma_L, \sigma_H) = (1.02249)\sigma_H - (0.354779)\sigma_L - 18.9121 \tag{4.65a}$$

$$f(r, \theta, z) = r[(0.973878)\cos\theta + (0.272593)\sin\theta] + (0.385505)z - 18.9121\,, \tag{4.65b}$$

However, the flow potential for deviatoric associativity changes to

$$g(\sigma_L, \sigma_H) = (0.901250)\sigma_H - (0.476067)\sigma_L - (0.121288)\sigma_M \tag{4.66a}$$

$$g(r, \theta, z) = r[(0.973878)\cos\theta + (0.272593)\sin\theta] + (0.175428)z \tag{4.66b}$$

Unlike Eq. 4.47 for consistent non-associativity, the flow potential for deviatoric associativity in Eq. 4.66 *depends on the middle eigenvalue* even though the yield function itself does not.

The change in the flow rule results in plastic loading at vertex states. The exact solution for this new problem is shown in Table 4.11. Each leg's name ends in E, PF, or PV to indicate whether the leg (or sub-leg) is elastic, plastic on a yield surface flat, or plastic at a yield vertex. After presenting this exact solution in tabular and graphical form, we will clarify some of the details of the solution procedure by showing the calculations for the plastic part of Leg 3. The eigenvalue ordering indicated the first column of Table 4.9 following the same notation as used in Example 1.

Table 4.11: Exact Solution (deviatoric associativity)

Leg	end time	reason for ending leg	ε_{11} (10^{-3}) at end	ε_{22} (10^{-3}) at end	ε_{33} (10^{-3}) at end	σ_{11} at end	σ_{33} at end
1E (LLH)	0.1	change in prescribed strain rate	–0.8	–0.8	0.56216	–33.5135	–33.5135
2E (MLH)	0.2	change in prescribed strain rate	0.3	–1.2	0.31622	–0.39897	–37.3037
3E (MLH)	0.21719	yield	0.3	–1.68133	0.48533	–4.55972	–53.3066
3PF (MLH)	0.239175	vertex	0.3	–2.2969	1.53999	0	–53.3066
3PV (HLH)	0.3	change in prescribed strain rate	0.3	–4.0	4.33009	0	–53.3066
4E (MLH)	0.4	change in prescribed strain rate	–1.0	–3.5	4.61117	–38.8996	–47.9205
5E (MLH) (LMH)	0.412345	yield	–1.48147	–3.31482	4.71528	–53.3066	–45.9257
5PF (LMH)	0.475692	vertex	–3.95198	–2.36462	8.27765	–53.3066	0
5PV (LHH)	0.5	change in prescribed strain rate	–4.9	–2.0	9.46613	–53.3066	0
6E (LMH) (MLH)	0.592145	yield	–3.97855	–3.8429	9.78988	–38.6013	–53.3066
6PF (MLH)	0.6	change in prescribed strain rate	–3.9	–4.0	10.0036	–35.1540	–53.3066
7E (MLH) (LMH) (LHM)	0.698527	yield	–3.9	–2.02946	9.31127	–18.1199	12.2089
7PF (LHM)	0.7	change in prescribed strain rate	–3.9	–2.0	9.30179	–17.6151	12.384

The exact solution is graphed in Fig. 4.9. The corresponding exact solutions for the Lode coordinates are shown in Fig. 4.10. The first leg is biaxial compression, which is a form of triaxial extension (Lode angle 30°) because it tends to increase the length to diameter ratio of axisymmetric specimens.

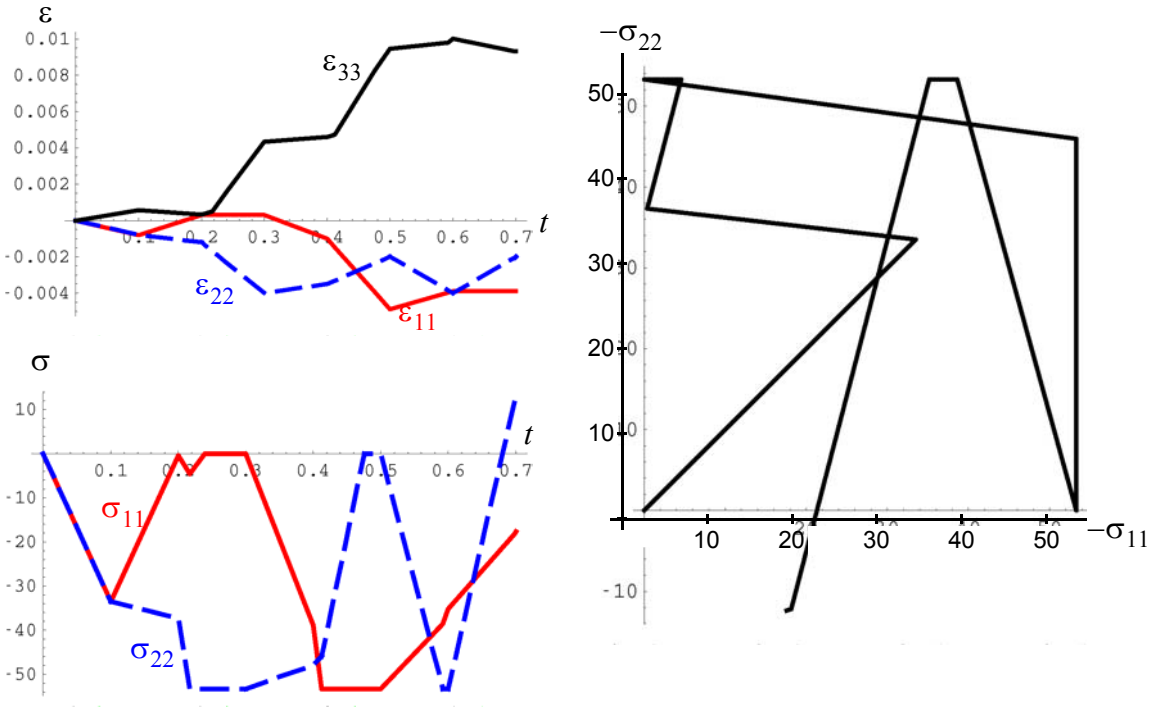

Figure 4.12. Exact plane stress solution for the in-plane stress history and out-of-plane strain history corresponding to the in-plane driving strains prescribed in Table 4.7. The stress diagram shows the analytical solution (thick orange line) overlaid with a numerical solution (thin black line) from the Sandia GeoModel [16].

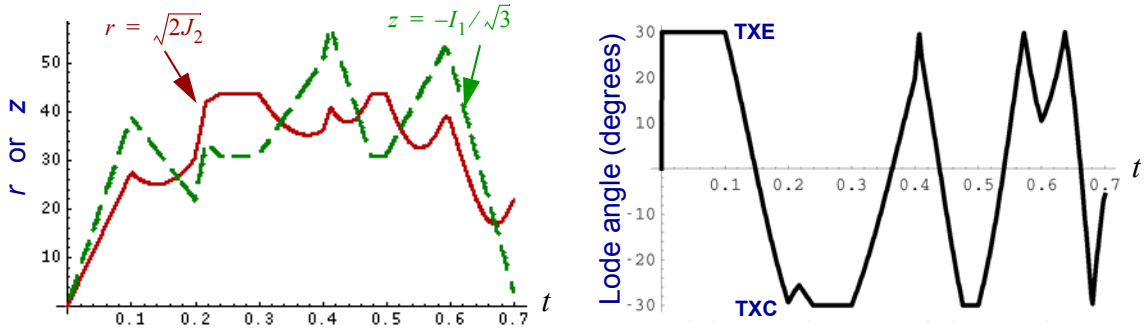

Figure 4.13. Exact solution for Lode coordinates. In this manuscript, the Lode angle is defined to be positive in triaxial extension (TXE) and negative in triaxial compression (TXC).

This concludes our presentation of the exact solution. We will now provide some details of the analysis by showing the actual computations associated with Leg 3. Computations associated with the other plastic legs are similar.

Detailed analysis of leg 3. To illustrate how this problem was solved, we will consider Leg 3, which is responsible for the odd-looking "hook" in the stress plot of Fig. 4.12. Leg 3 begins at time t=0.2 and ends at time t=0.3. After analyzing legs 1 and 2 (both of which are entirely elastic), the initial state (at time t=0.2) for Leg 3 is

$$\underset{\sim}{\sigma}^{(t=0.2)} = \text{DIAG}[-0.39897, -37.3037, 0] \tag{4.67a}$$

$$\underset{\sim}{\varepsilon}^{(t=0.2)} = \text{DIAG}[0.0003, -0.0012, 0.000316216] \tag{4.67b}$$

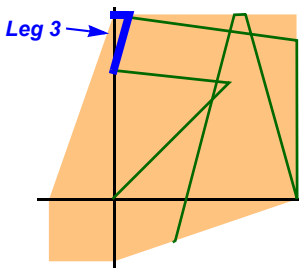

Figure 4.14. Leg 3.

Throughout Leg 3, the prescribed in-plane strain rates are

$$\dot{\varepsilon}_1 = 0 \qquad \text{and} \qquad \dot{\varepsilon}_2 = -0.028 \tag{4.68}$$

Of course, for plane stress, the $\sigma_3 = 0$ and therefore

$$\dot{\sigma}_3 = 0 \tag{4.69}$$

The unknowns in the analysis are $\dot{\sigma}_1$, $\dot{\sigma}_2$, and $\dot{\varepsilon}_3$. This leg, we will show, begins elastically, loads plastically on a single yield plane, and then finishes at a yield vertex.

When the stress is away from vertices, the exact solution during plastic loading is found by applying Eq. (2.39) to obtain $\dot{\varepsilon}_3$ and then Eqs. (2.25a) and (2.25b) for $\dot{\sigma}_1$ and $\dot{\sigma}_2$:

$$\dot{\varepsilon}_3 = \frac{\lambda(\dot{\varepsilon}_1 + \dot{\varepsilon}_2) - \frac{1}{\eta}P_3(Q_1\dot{\varepsilon}_1 + Q_2\dot{\varepsilon}_2)}{\frac{1}{\eta}P_3Q_3 - (2G + \lambda)} \tag{4.70a}$$

$$\dot{\sigma}_1 = 2G\dot{\varepsilon}_1 + \lambda(\dot{\varepsilon}_1 + \dot{\varepsilon}_2 + \dot{\varepsilon}_3) - \frac{1}{\eta}P_1(Q_1\dot{\varepsilon}_1 + Q_2\dot{\varepsilon}_2 + Q_3\dot{\varepsilon}_3) \tag{4.70b}$$

$$\dot{\sigma}_2 = 2G\dot{\varepsilon}_2 + \lambda(\dot{\varepsilon}_1 + \dot{\varepsilon}_2 + \dot{\varepsilon}_3) - \frac{1}{\eta}P_2(Q_1\dot{\varepsilon}_1 + Q_2\dot{\varepsilon}_2 + Q_3\dot{\varepsilon}_3) \tag{4.70c}$$

The yield surface normal is parallel to the yield function gradient,

$$\frac{df}{d\underset{\sim}{\sigma}} = \frac{\partial f}{\partial \sigma_L}\underset{\sim}{\boldsymbol{e}}_L + \frac{\partial f}{\partial \sigma_H}\underset{\sim}{\boldsymbol{e}}_H \tag{4.71}$$

Here, $\underset{\sim}{\boldsymbol{e}}_L$ is the unit "eigenprojector" tensor that equals zero in every component except for a 1 at the location of the lowest principal stress. The eigenprojector $\underset{\sim}{\boldsymbol{e}}_H$ similarly demarks the location of the highest principal stress. Using Eq. (4.65) to compute the yield function derivatives in Eq. (4.71), and then normalizing the result gives the formula for the unit normal of the yield surface:

$$\underset{\sim}{\boldsymbol{N}} = (-0.3278)\underset{\sim}{\boldsymbol{e}}_L + (0.9447)\underset{\sim}{\boldsymbol{e}}_H \tag{4.72}$$

Similarly, the unit tensor parallel to the plastic flow direction is

$$\underset{\sim}{\boldsymbol{M}} = (-0.4638)\underset{\sim}{\boldsymbol{e}}_L + (-0.1182)\underset{\sim}{\boldsymbol{e}}_M + (0.8780)\underset{\sim}{\boldsymbol{e}}_H \tag{4.73}$$

The $\underset{\sim}{P}$ and $\underset{\sim}{Q}$ tensors equal the elastic stiffness operating on $\underset{\sim}{M}$ and $\underset{\sim}{N}$ respectively. Hence,

$$\underset{\sim}{P} = 2G\underset{\sim}{M} + \lambda(\mathrm{tr}\underset{\sim}{M})\underset{\sim}{I} \qquad \text{and} \qquad \underset{\sim}{Q} = 2G\underset{\sim}{N} + \lambda(\mathrm{tr}\underset{\sim}{N})\underset{\sim}{I} \tag{4.74}$$

Of course $\underset{\sim}{I} = \mathrm{DIAG}[1, 1, 1]$. The trace is, as usual, the sum of diagonal components, so it is unaffected by eigenvalue ordering. Therefore, substituting Eqs. 4.72 and 4.73 into 4.74 gives

$$\underset{\sim}{P} = (-7466.2)\underset{\sim}{\mathcal{E}}_L + (1037.8)\underset{\sim}{\mathcal{E}}_M + (25547.1)\underset{\sim}{\mathcal{E}}_H \tag{4.75a}$$

$$\underset{\sim}{Q} = (-156.86)\underset{\sim}{\mathcal{E}}_L + (8221.8)\underset{\sim}{\mathcal{E}}_M + (31465.6)\underset{\sim}{\mathcal{E}}_H \tag{4.75b}$$

Regardless of eigenvalue ordering, the η scalar is given by

$$\eta = \underset{\sim}{N}:\underset{\sim}{P} = 26583 \tag{4.76}$$

Trial elastic solution (valid until the yield function becomes positive)

As usual, the analysis begins by assuming elasticity. During elastic loading, the solution is obtained by evaluating Eq. 4.70, with the P_k's set to zero:

$$\dot{\varepsilon}_3 = \frac{\lambda(\dot{\varepsilon}_1 + \dot{\varepsilon}_2)}{-(2G + \lambda)} = \frac{(13326.7)[(-0.028) + 0]}{-(37929.9)} = 0.009838 \tag{4.77a}$$

$$\dot{\sigma}_1 = 2G\dot{\varepsilon}_1 + \lambda(\dot{\varepsilon}_1 + \dot{\varepsilon}_2 + \dot{\varepsilon}_3) = 2(12301.6)(-0.028) + (13326.7)[-0.028 + 0 + 0.009838] = -242.0 \tag{4.77b}$$

$$\dot{\sigma}_2 = 2G\dot{\varepsilon}_2 + \lambda(\dot{\varepsilon}_1 + \dot{\varepsilon}_2 + \dot{\varepsilon}_3) = 2(12301.6)(0.0000) + (13326.7)[-0.028 + 0 + 0.009838] = -930.9 \tag{4.77c}$$

These constant rates apply during the entirety of the elastic loading phase. Therefore integrating these rates using the initial conditions in Eq. 4.67 gives the time varying solution:

$$\varepsilon_3 = \varepsilon_3^{\text{initial}} + \dot{\varepsilon}_3(t - t^{\text{initial}}) = 0.000316216 + (0.009838)(t - 0.2) \tag{4.78a}$$

$$\sigma_1 = \sigma_1^{\text{initial}} + \dot{\sigma}_1(t - t^{\text{initial}}) = -0.39897 + (-242.0)(t - 0.2) \tag{4.78b}$$

$$\sigma_2 = \sigma_2^{\text{initial}} + \dot{\sigma}_2(t - t^{\text{initial}}) = -37.3037 + (-930.9)(t - 0.2) \tag{4.78c}$$

A plot of the time varying solution is shown in Fig. 4.15, where it is evident that the eigenvalue ordering is

$$\sigma_H = \sigma_3\,, \quad \sigma_M = \sigma_1\,, \quad \sigma_L = \sigma_2 \tag{4.79}$$

Substituting these into Eq. (4.65) gives the time-varying value of the yield function:

$$f = -66.2481 + 305.161t$$

The yield function is negative from the start time, $t = 0.2$, up until the yield time

$$t^{\text{yield}} = 0.2172\,.$$

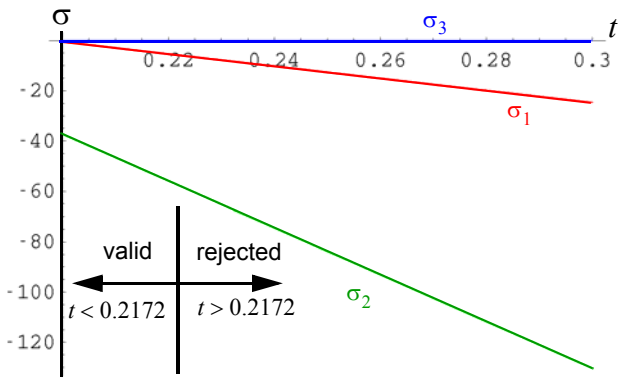

Figure 4.15. Trial elastic solution for leg 3. This solution is valid until time t^{yield} when the yield function becomes zero.

The trial elastic solution in Eq. 4.78 is therefore valid up through the yield time.

Single surface plasticity solution (valid until the stress reaches a yield vertex)

The initial state for the plastic loading leg is obtained by evaluating Eq. (4.78) at $t = t^{\text{yield}}$:

$$\underset{\sim}{\sigma}^{(t=0.2172)} = \text{DIAG}[-4.560, -53.31, \quad 0] \tag{4.80a}$$

$$\underset{\sim}{\varepsilon}^{(t=0.2172)} = \text{DIAG}[0.0003, -0.001681, 0.0004853] \tag{4.80b}$$

The eigenvalues of the stress are initially all distinct, which means that the state is not initially at a yield surface vertex. Therefore, the single-surface plasticity solution in Eq. (4.70) either through the end of the leg or until a vertex is reached (where eigenvalue ordering changes). Because the high stress eigenvalue is σ_3, the eigenprojector $\underset{\sim}{e}_H$ is zeros everywhere except a 1 in the 33 component. Because the middle eigenvalue is σ_1, the eigenprojector $\underset{\sim}{e}_M$ has a 1 in the 11 component and zeros elsewhere. Similarly, because σ_2 is the low eigenvalue, $\underset{\sim}{e}_L$ has a 1 in the 22 location. To summarize,

$$\underset{\sim}{e}_L = \text{DIAG}[0, 1, 0]\,, \qquad \underset{\sim}{e}_M = \text{DIAG}[1, 0, 0]\,, \qquad \underset{\sim}{e}_H = \text{DIAG}[0, 0, 1] \tag{4.81}$$

Using, respectively, Eqs. (4.73) and (4.72), the unit flow direction and yield normal are

$$\underset{\sim}{M} = (-0.4638)\underset{\sim}{\varepsilon}_L + (-0.1182)\underset{\sim}{\varepsilon}_M + (0.8780)\underset{\sim}{\varepsilon}_H = \text{DIAG}[-0.1182, -0.4638, 0.8780] \tag{4.82a}$$

$$\underset{\sim}{N} = (-0.3278)\underset{\sim}{\varepsilon}_L + (0.9447)\underset{\sim}{\varepsilon}_H = \text{DIAG}[0, -0.3278, 0.9447] \tag{4.82b}$$

Using Eq. (4.75), the $\underset{\sim}{P}$ and $\underset{\sim}{Q}$ tensors are

$$\underset{\sim}{P} = (-7466.2)\underset{\sim}{\varepsilon}_L + (1037.8)\underset{\sim}{\varepsilon}_M + (25547.1)\underset{\sim}{\varepsilon}_H = \text{DIAG}[1037.8, -7466.2, 25547.1] \tag{4.83a}$$

$$\underset{\sim}{Q} = (-156.86)\underset{\sim}{\varepsilon}_L + (8221.8)\underset{\sim}{\varepsilon}_M + (31465.6)\underset{\sim}{\varepsilon}_H = \text{DIAG}[8221.8, -156.86, 31465.6] \tag{4.83b}$$

The η scalar is given by

$$\eta = \underset{\sim}{N}:\underset{\sim}{P} = 26583 \tag{4.84}$$

Of course, the prescribed strain rates $\dot{\varepsilon}_1$ and $\dot{\varepsilon}_2$ are the same as they were during the elastic leg. Hence, applying Eqs. (4.70), the single-surface plasticity solution, valid after time $t = t^{\text{yield}}$, is

$$\dot{\varepsilon}_3 = \frac{\lambda(\dot{\varepsilon}_1 + \dot{\varepsilon}_2) - \frac{1}{\eta}P_3(Q_1\dot{\varepsilon}_1 + Q_2\dot{\varepsilon}_2)}{\frac{1}{\eta}P_3Q_3 - (2G + \lambda)}$$

$$= \frac{(13327)(0 - 0.028) - \frac{1}{26583}(25547.1)[(8221.8)(0) + (-156.86)(-0.028)]}{\frac{1}{26583}(25547.1)31465.6 - (37930)}$$

$$= 0.04797 \tag{4.85a}$$

$$\dot{\sigma}_1 = 2G\dot{\varepsilon}_1 + \lambda(\dot{\varepsilon}_1 + \dot{\varepsilon}_2 + \dot{\varepsilon}_3) - \frac{1}{\eta}P_1(Q_1\dot{\varepsilon}_1 + Q_2\dot{\varepsilon}_2 + Q_3\dot{\varepsilon}_3) = 207.4 \tag{4.85b}$$

$$\dot{\sigma}_2 = 2G\dot{\varepsilon}_2 + \lambda(\dot{\varepsilon}_1 + \dot{\varepsilon}_2 + \dot{\varepsilon}_3) - \frac{1}{\eta}P_2(Q_1\dot{\varepsilon}_1 + Q_2\dot{\varepsilon}_2 + Q_3\dot{\varepsilon}_3) = 0.00 \tag{4.85c}$$

These rates may be integrated through time using Eq. (4.80) as the initial condition. The resulting stress histories, shown in Fig. 4.16, reveal that two eigenvalues become equal at time $t^{\text{swap}} = 0.2392$, which marks the point at which this solution is no longer valid. If you (wrongly) presumed the solution in Fig. 4.16 valid beyond the swap time, then you would find that it violates the yield condition (i.e., it produces stress states for which $f > 0$).

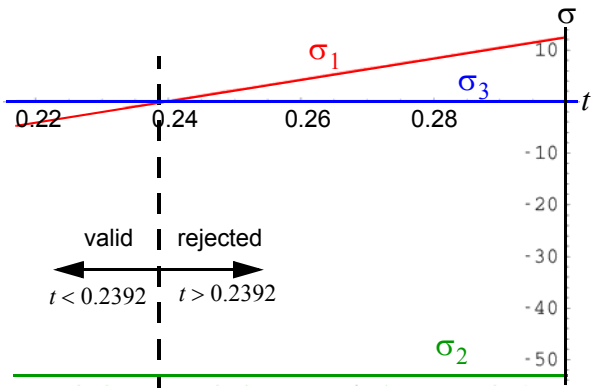

Figure 4.16. Single-surface plasticity solution applicable from the onset of yield until the eigenvalues swap ordering.

Demonstrating that the stress does not move past the vertex

The stress is at a vertex when two stress eigenvalues become equal (and the stress is at yield). Two possibilities exist: either the stress will dwell at the vertex, or it will move beyond the vertex into a different yield surface flat. If the total strain rate were known, determining which one of these two possibilities applies would be a simple matter of using STEP __ of the vertex instructions on page __ of the Radial Return monograph. Unfortunately, however, the trial stress rate is *not* the same as the stress rate found earlier during the elastic leg of this solution, which enforced the plane-stress boundary condition. The trial stress rate in the vertex instructions must equal the stiffness operating on the total strain rate, but the out-of-plane strain rate $\dot{\varepsilon}_3$ is not known for this problem. To get around this issue, one must tentatively assume that the stress will pass beyond the vertex. Then a single-surface plasticity analysis is performed similar to what was shown above except with $\overset{\varrho}{\approx}_M$ and $\overset{\varrho}{\approx}_H$ trading roles. The resulting solution is easily shown to violate the yield condition. Hence, the only remaining possibility is two-surface vertex analysis.

Given that the trial stress rate must point into the Koiter fan, apply two-surface vertex theory.

To find the stress solution beyond t^{swap}, we must obtain the tangent stiffness tensor in STEP __ of the vertex instructions in the Radial Return document:

$$\underset{\approx}{\underset{\approx}{\boldsymbol{T}}} = \underset{\approx}{\underset{\approx}{\boldsymbol{E}}} - \sum_{j=1}^{n}\sum_{k=1}^{n} \eta_{jk}^{-1} \underset{\approx}{\boldsymbol{P}}_j \underset{\approx}{\boldsymbol{Q}}_k \tag{4.86}$$

For fixed-axes loading, this fourth-order tensor may be recast as a 3×3 matrix. Of course, for fixed-axes loading, the elastic stiffness is

$$[E] = \begin{bmatrix} 2G+\lambda & \lambda & \lambda \\ \lambda & 2G+\lambda & \lambda \\ \lambda & \lambda & 2G+\lambda \end{bmatrix} = \begin{bmatrix} 37930 & 13327 & 13327 \\ 13327 & 37930 & 13327 \\ 13327 & 13327 & 37930 \end{bmatrix} \tag{4.87}$$

Computing the last term in Eq. 4.86 is the most difficult part of vertex analysis.

According to STEP __ of the vertex instructions, the η_{ij} matrix (which is analogous to the η parameter used in single-surface plasticity) is given by

$$\eta_{ij} \equiv \underset{\approx}{\boldsymbol{N}}_i : \underset{\approx}{\boldsymbol{P}}_j \tag{4.88}$$

This is a non-hardening yield problem, so the ensemble hardening moduli H_{ij} have been set to zero. The vertex for this problem is the one where the high and middle eigenvalues swap places. It is a triaxial extension (TXE) vertex. In the single-surface solution derived earlier, the high and middle eigenvalues were located in the first and third positions of the stress array. The first active yield normal is the one that applied before t^{swap}. The second active yield normal is the same except with the first and third components exchanged:

$$\underset{\approx}{\boldsymbol{N}}_1 = \text{DIAG}[0, -0.3278, 0.9447] \quad \text{and} \quad \underset{\approx}{\boldsymbol{N}}_2 = \text{DIAG}[0.9447, -0.3278, 0] \tag{4.89}$$

Likewise, the two active projection direction tensors are

$$\underset{\approx}{\boldsymbol{P}}_1 = \text{DIAG}[1037.8, -7466.2, 25547.1] \quad \text{and} \quad \underset{\approx}{\boldsymbol{P}}_2 = \text{DIAG}[25547.1, -7466.2, 1037.8] \tag{4.90}$$

and the two active Q-tensors are

$$\underset{\approx}{\boldsymbol{Q}}_1 = \text{DIAG}[8221.8, -156.86, 31465.6] \quad \text{and} \quad \underset{\approx}{\boldsymbol{Q}}_2 = \text{DIAG}[31465.6, -156.86, 8221.8] \tag{4.91}$$

Applying Eq. 4.88,

$$[\eta] = \begin{bmatrix} (\underset{\approx}{N}_1 : \underset{\approx}{P}_1) & (\underset{\approx}{N}_1 : \underset{\approx}{P}_2) \\ (\underset{\approx}{N}_2 : \underset{\approx}{P}_1) & (\underset{\approx}{N}_2 : \underset{\approx}{P}_2) \end{bmatrix} = \begin{bmatrix} 26583 & 3428 \\ 3428 & 26583 \end{bmatrix} \tag{4.92}$$

whose inverse is

$$[\eta]^{-1} = \begin{bmatrix} 38.254 & -4.9330 \\ -4.9330 & 38.254 \end{bmatrix} \times 10^{-6} \tag{4.93}$$

Incidentally, this $[\eta]$ matrix happens to be symmetric and have equal diagonal components only because of the nice symmetries of the Mohr-Coulomb model. For more general vertices (such as found in two-surface cap plasticity), the $[\eta]$ matrix can potentially have all distinct components.

Computing the last term in Eq. (4.86) requires recognizing that each $\underset{\approx}{P}_j \underset{\approx}{Q}_k$ is a dyadic multiplication. For fixed axes loading, the result can be saved as a 3×3 matrix whose rs component is given by $(\underset{\approx}{P}_j)_r (\underset{\approx}{Q}_k)_s$. For example,

$$[\underset{\sim}{P}_1 \underset{\sim}{Q}_2] = \begin{bmatrix} (\underset{\sim}{P}_1)_1 (\underset{\sim}{Q}_2)_1 & (\underset{\sim}{P}_1)_1 (\underset{\sim}{Q}_2)_2 & (\underset{\sim}{P}_1)_1 (\underset{\sim}{Q}_2)_3 \\ (\underset{\sim}{P}_1)_2 (\underset{\sim}{Q}_2)_1 & (\underset{\sim}{P}_1)_2 (\underset{\sim}{Q}_2)_2 & (\underset{\sim}{P}_1)_2 (\underset{\sim}{Q}_2)_3 \\ (\underset{\sim}{P}_1)_3 (\underset{\sim}{Q}_2)_1 & (\underset{\sim}{P}_1)_3 (\underset{\sim}{Q}_2)_2 & (\underset{\sim}{P}_1)_3 (\underset{\sim}{Q}_2)_3 \end{bmatrix}$$

$$= \begin{bmatrix} (1037.8)(31465.6) & (1037.8)(-156.86) & (1037.8)(8221.8) \\ (-7466.2)(31465.6) & (-7466.2)(-156.86) & (-7466.2)(8221.8) \\ (25547.1)(31465.6) & (25547.1)(-156.86) & (25547.1)(8221.8) \end{bmatrix}$$

$$= \begin{bmatrix} 32.66 & 0.1628 & 8.533 \\ -234.9 & -1.171 & -61.39 \\ 803.9 & 4.007 & 210.0 \end{bmatrix} \times 10^6 \tag{4.94}$$

Continuing similarly, to compute all of the terms in the double sum of Eq. 4.86, the tangent stiffness tensor is ultimately found to be

$$\left[\underset{\sim}{\underset{\sim}{T}}\right] = \begin{bmatrix} 8049.9 & 13188 & 8049.9 \\ 23200 & 38008 & 23200 \\ 8049.9 & 13188 & 8049.9 \end{bmatrix} \tag{4.95}$$

The governing equation,

$$\dot{\underset{\approx}{\sigma}} = \underset{\approx\approx}{T} : \dot{\underset{\approx}{\varepsilon}}, \tag{4.96}$$

can be written as a 3×3 system in which there are three unknowns, $\dot{\sigma}_1$, $\dot{\sigma}_2$, and $\dot{\varepsilon}_3$. Specifically, we know for plane stress that $\dot{\sigma}_3 = 0$. During this leg, we also know that $\dot{\varepsilon}_1 = 0$ and $\dot{\varepsilon}_2 = -0.028$. Therefore, the matrix form of Eq. (4.96) is

$$\begin{bmatrix} \dot{\sigma}_1 \\ \dot{\sigma}_2 \\ 0 \end{bmatrix} = \begin{bmatrix} 8049.9 & 13188 & 8049.9 \\ 23200 & 38008 & 23200 \\ 8049.9 & 13188 & 8049.9 \end{bmatrix} \begin{bmatrix} 0 \\ -0.028 \\ \dot{\varepsilon}_3 \end{bmatrix} \tag{4.97}$$

Solving this system for the unknowns gives the final solution:

$$\dot{\sigma}_1 = 0, \qquad \dot{\sigma}_2 = 0, \qquad \text{and} \qquad \dot{\varepsilon}_3 = 0.04587 \tag{4.98}$$

In other words, once the vertex has been reached, the stress remains constant. This result is not as self-evident as one might think — vertex loading on a TXE vertex requires only that the stress must remain TXE, but it does not require the stress to remain constant (in general, the pressure can change even though it remained constant *for this particular example*). The out-of-plane strain component grows over time at a faster rate than it did during the single-surface plastic loading phase. To summarize, Fig. 4.17 shows the combined three-stage histories of the stress and strain applicable over leg 3.

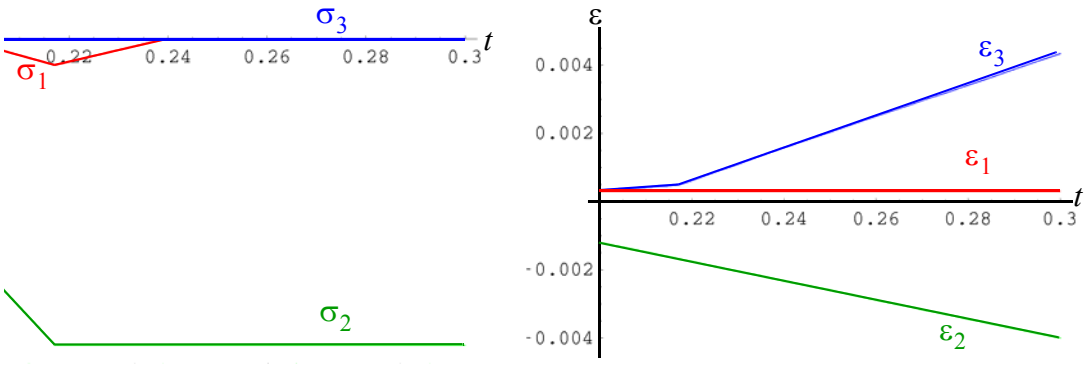

Figure 4.17. Stress and strain histories over leg 3.

This concludes our detailed analysis of Leg 3. Other legs are analyzed similarly.